Analysis of Stability and Dispersion in a Finite Element Method for Debye and Lorentz Dispersive Media

H. T. Banks*
Center for Research in Scientific Computation
North Carolina State University
Raleigh, NC 27695-8205

V. A. Bokil† and N. L. Gibson‡
Department of Mathematics
Oregon State University
Corvallis, OR 97331-4605

December 19, 2006

Abstract:

We study the stability properties of, and the phase error present in, a finite element scheme for Maxwell's equations coupled with a Debye or Lorentz polarization model. In one dimension we consider a second order formulation for the electric field with an ordinary differential equation for the electric polarization added as an auxiliary constraint. The finite element method uses linear finite elements in space for the electric field as well as the electric polarization, and a theta scheme for the time discretization. Numerical experiments suggest the method is unconditionally stable for both Debye and Lorentz models. We compare the stability and phase error properties of the method presented here with those of finite difference methods that have been analyzed in the literature. We also conduct numerical simulations that verify the stability and dispersion properties of the scheme.

Keywords: Maxwell's Equations, Debye, Lorentz, Finite Elements, FDTD, dissipation, dispersion.

*email: htbanks@ncsu.edu
†email: bokilv@math.oregonstate.edu
‡email: gibsonn@math.oregonstate.edu

1 Introduction

Noninvasive interrogation of the interior of tissues and other materials by electromagnetic waves has important applications in various fields including medical imaging for the early detection of anomalies and nondestructive damage detection in aircraft [2, 3]. For example, microwave imaging for breast cancer detection is expected to be safe for the patient and has the potential to detect very small cancerous tumors in the breast [17]. This ability for detection is based on the difference in electrical properties of malignant and normal tissues. Biological tissue interactions with the fields are defined by their complex permittivity which is a function of the various electric and magnetic polarization mechanisms and conductivity of the biological medium. Similarly, nondestructive damage detection in materials for the detection of defects such as cracks is based upon the changes in the electrical properties that occur due to the presence of these defects. Thus, one of the aims of electromagnetic interrogation problems is the determination of the dielectric properties of the materials under investigation.

To computationally simulate these electromagnetic interrogation problems requires setting up a suitable inverse problem which involves numerous forward simulations of the propagation of transient electromagnetic waves in lossy dispersive dielectrics such as biological tissue. Hence, the development of accurate, consistent and stable discrete forward solvers is very important, as errors in the numerical solvers can result in inaccurate determination of the dielectric properties that determine the characteristics of the material being investigated.

The electric and magnetic fields inside a material are governed by the macroscopic Maxwell's equations along with constitutive laws that account for the response of the material to the electromagnetic field. In special cases Maxwell's equations can be reduced to a vector wave equation in the electric or magnetic fields. Numerical approximation algorithms of time-dependent wave equations and Maxwell's equations introduce error into the amplitude and speed of the propagating waves. These errors include *dissipation*, the dampening of some frequency modes, and *dispersion*, the frequency dependence of the phase velocity of numerical wave modes in the computational grid.

Dielectric materials have actual physical dispersion. The complex electric permittivity of a dielectric medium is frequency dependent (has dielectric dispersion). Thus, an appropriate discretization method should have a numerical dispersion that matches the model dispersion as closely as possible. Dielectric materials also have physical dissipation, or attenuation, which must also be correctly computed by a numerical method. In particular, if a method does not sufficiently damp initial disturbances, possibly due to round-off error, the method can become unstable. Certain algorithms have criteria based on discretization parameters to determine when it may be unstable; these are called *conditionally stable methods*.

The stability and dispersion properties for the finite difference time domain (FDTD) schemes applied to Maxwell's equations in free space are well known (see [37]). Additionally, different time domain finite element methods have also been devised for the numerical approximation of Maxwell's equations in free space (see [28, 24] and the references therein). While free space analyses for finite element and finite difference methods are well documented, stability and phase error analysis for dispersive dielectrics has been primarily focused on finite difference methods (see [29, 37] for standard second order methods and

[30] for higher order schemes). The treatment for finite element methods has been limited to scalar-potential formulations to model dielectric dispersion at low frequencies ([32]), scalar Helmholtz equation ([25]), and in some cases, hybrid methods ([16]).

There are several FDTD extensions that have been developed to model electromagnetic pulse propagation in dispersive media. One technique is to add to Maxwell's equations a set of ODE's that relate the electric displacement $\vec{D}(t)$ to the electric field $\vec{E}(t)$ [19], or a set of ODE's that model the dynamic evolution of the macroscopic polarization vector $\vec{P}(t)$ driven by the electric field [21, 20]. Dielectric dispersion can be expressed in the time domain as a convolution integral involving the electric field and a causal susceptibility function. The recursive convolution method [27, 26, 22] uses a recursive technique to update the convolution representation of the constitutive law along with the FDTD time update of Maxwell's equations. There are other methods such as the Z-transform [35, 34] and the TLM method [10] that have also been used to model pulse propagation in dispersive media. Many of these methods have been compared and analyzed for their numerical errors and stability properties [29, 38, 31, 11, 13].

In this paper we study the properties of the discretized Maxwell's equations with Debye or Lorentz polarization, using a finite element method, in terms of numerical stability and dispersion analyses. We obtain information about the expected accuracy of the method from the construction of the dispersion relation which relates the numerical wave number k to the frequency ω for waves propagating in the finite element grid and then compare with the dispersion relation for the corresponding continuous model (differential equations). We compare the stability and dispersion properties of the finite element method with those of finite difference methods analyzed in [29]. Such finite element methods have been used for the electromagnetic interrogation of dielectric media with a metal backing, for the determination of dielectric properties and geometrical dimensions of the medium [6], as well as for the detection of cracks in composite materials [9]. In [1], finite element methods were used to interrogate dielectric media with acoustic waves as virtual reflectors.

We analyze one dimensional models to which we apply standard linear finite elements for the spatial discretization of the electric field and the polarization. Maxwell's equations are reduced to a wave equation in the electric field, and the constitutive law in the medium involves an ordinary differential equation that describes the dynamic evolution of the polarization driven by the electric field. The entire system is rewritten in first order form and time discretized using a theta scheme.

The numerical stability results for Debye and Lorentz media suggest that the extension of the finite element scheme for these media retain the unconditional stability property of the scheme in free space. The well known Lax-Richtmyer theorem [33] states that the convergence of consistent difference schemes to initial value problems represented by PDE's is equivalent to stability. Thus, unconditional stability is a desirable property of temporal discretization schemes as it allows the choice of the time step to be determined by the physical dimensions of the problem, such as a relaxation time. The FDTD methods, on the other hand, are conditionally stable. Since the stability condition is determined by the smallest cell size in the domain, the FDTD analysis of very fine geometric structures requires a large number of time iterations. In the finite element case unconditional stability allows us to choose the *Courant number*, which relates the time step to the mesh step size, to minimize the numerical phase error.

The numerical dispersion analysis shows that for accuracy we need to resolve the shortest time scale in the problem which agrees with the result obtained in [29]. This is reflected in the fact that the time step for simulating Debye media should be chosen to be about $O(10^{-3})\tau$, where τ is the relaxation time of the medium, whereas for Lorentz media, the time step should be chosen to be the minimum of $O(10^{-2})\tau$ and $O(10^{-2})(\frac{2\pi}{\omega_0})$, where ω_0 is the resonance frequency of the medium.

We thus determine a guideline for users in which the time step is chosen to minimize the dissipation of the scheme and the Courant factor is chosen to minimize the phase error, providing good agreement between the exact and numerical complex permittivity.

In this paper we present finite element schemes for discretizing Maxwell's equations coupled with a Debye or Lorentz polarization model. We analyze the stability and dispersion properties, and compare these to results for FDTD schemes. Finally, we present simulations to validate our results.

2 Model formulation

We consider Maxwell's equations which govern the electric field $\vec{E}$ and the magnetic field $\vec{H}$ in a domain Ω from time 0 to T given as

$$\frac{\partial \vec{D}}{\partial t} + \vec{J} - \nabla \times \vec{H} = 0 \text{ in } (0,T) \times \Omega, \tag{2.1a}$$

$$\frac{\partial \vec{B}}{\partial t} + \nabla \times \vec{E} = 0 \text{ in } (0,T) \times \Omega, \tag{2.1b}$$

$$\nabla \cdot \vec{D} = 0 \text{ in } (0,T) \times \Omega, \tag{2.1c}$$

$$\nabla \cdot \vec{B} = 0 \text{ in } (0,T) \times \Omega, \tag{2.1d}$$

$$\vec{E}(0,\vec{x}) = 0 \text{ in } \Omega, \tag{2.1e}$$

$$\vec{H}(0,\vec{x}) = 0 \text{ in } \Omega. \tag{2.1f}$$

The fields $\vec{D}, \vec{B}$ are the electric and magnetic flux densities respectively. All the fields in (2.1) are functions of position $\vec{x} = (x, y, z)$ and time t. We have $\vec{J} = \vec{J_c} + \vec{J_s}$, where $\vec{J_c}$ is a conduction current density and $\vec{J_s}$ is the source current density. However, we will assume $\vec{J_c} = 0$ in this paper, as we are interested in dielectrics with no free charges. Appropriate boundary conditions are added to system (2.1) to terminate the computational domain.

Constitutive relations which relate the electric and magnetic fluxes $\vec{D}, \vec{B}$ to the electric and magnetic fields $\vec{E}, \vec{H}$ are added to these equations to make the system fully determined and to describe the response of a material to the electromagnetic fields. In free space, these constitutive relations are $\vec{D} = \epsilon_0 \vec{E}$, and $\vec{B} = \mu_0 \vec{H}$, where ϵ_0 and μ_0 are the permittivity and the permeability of free space, respectively, and are constant [18]. In general there are different possible forms for these constitutive relationships. In a frequency domain formulation of Maxwell's equations, these are usually converted to linear relationships between the dependent and independent quantities with frequency dependent coefficient parameters. We will consider the case of a dielectric in which magnetic effects are negligible. Thus, within the dielectric medium we have constitutive relations that relate the flux densities $\vec{D}, \vec{B}$ to

the electric and magnetic fields, respectively, as

$$\vec{D} = \epsilon_0 \vec{E} + \vec{P}, \tag{2.2a}$$

$$\vec{B} = \mu_0 \vec{H}. \tag{2.2b}$$

In (2.2a), the quantity $\vec{P}$ is called the macroscopic electric polarization. (A discussion of the relationship between the macroscopic polarization and the microscopic material properties leading to distributions of relaxation times and other dielectric parameters in the constitutive laws can be found in [7].) Electric polarization may be defined as the electric field induced disturbance of the charge distribution in a region. This polarization may have an instantaneous component as well as delayed effects; the latter will usually have associated time constants called relaxation times which are denoted by τ. We define the instantaneous component of the polarization to be related to the electric field by means of a dielectric constant ϵ_0 and a susceptibility χ. The remainder of the electric polarization, called the relaxation polarization, is denoted as $\vec{P}_{\mathrm{R}}$. Therefore, we have

$$\vec{P} = \vec{P}_{\mathrm{I}} + \vec{P}_{\mathrm{R}} = \epsilon_0 \chi \vec{E} + \vec{P}_{\mathrm{R}}, \tag{2.3}$$

and hence the constitutive law (2.2a) becomes

$$\vec{D} = \epsilon_0 \epsilon_r \vec{E} + \vec{P}_{\mathrm{R}}, \tag{2.4}$$

where $\epsilon_r = (1 + \chi)$ is the relative permittivity of the dielectric medium. We will henceforth denote $\vec{P}_{\mathrm{R}}$ by $\vec{P}$, as the instantaneous polarization will be absorbed into the dielectric constant ϵ_r. The following section defines the equations for polarization models of interest in this paper.

2.1 Models for Polarization

To describe the behavior of the media's relaxation polarization $\vec{P}$, one may use ordinary differential equation models derived from those that consider microscopic polarization mechanisms such as dipole or orientational polarization (Debye), as well as ionic and electronic polarization (Lorentz), and other frequency dependent polarization mechanisms [4]. For more complex dielectric materials, a simple Debye or Lorentz polarization model is often not adequate to characterize the dispersive behavior of the material. One can then turn to combinations of Debye, Lorentz, or even more general n^{th} order mechanisms [6] as well as Cole-Cole type (fractional order derivative) models [12]. Additionally, materials may be represented by a distribution of the associated time constants or even a distribution of polarization mechanisms (see [8, 7]). In this report we concentrate our analysis on single pole Debye and Lorentz polarization models.

2.1.1 Debye Model

The macroscopic differential equation for the *Debye model* for *orientational* or *dipolar polarization* is given by

$$\tau \frac{\partial \vec{P}}{\partial t} + \vec{P} = \epsilon_0 (\epsilon_s - \epsilon_\infty) \vec{E}. \tag{2.5}$$

Here ϵ_s is the static relative permittivity. The presence of instantaneous polarization is accounted for in this case by the coefficient ϵ_∞ in the electric flux equation. That is, $\epsilon_r = \epsilon_\infty$. The electric polarization, less the part included in the instantaneous polarization, is seen to be a decaying exponential with relaxation parameter τ, which is driven by the electric field. This model was first proposed by Debye [15] to model the behavior of materials that possess permanent dipole moments. The magnitude of the polarization term $\vec{P}$ represents the degree of alignment of these individual moments and is based on a uniformity assumption at the molecular level (see [7]). The choice of coefficients in (2.5) gives a physical interpretation to ϵ_s and ϵ_∞ as the relative permittivities of the medium in the limit of the static field and very high frequencies, respectively. In the static case, we have $\vec{P}_t = 0$, so that $\vec{P} = \epsilon_0(\epsilon_s - \epsilon_\infty)\vec{E}$ and $\vec{D} = \epsilon_0\epsilon_s\vec{E}$. For very high frequencies, $\tau\vec{P}_t$ dominates $\vec{P}$ so that $\vec{P} \approx 0$ and $\vec{D} = \epsilon_0\epsilon_\infty\vec{E}$ (thus the notation of ∞).

The Debye model is most often used to model electromagnetic wave interactions with water-based substances, such as biological materials. In particular, biological tissue is well represented by multi-pole Debye models, by accounting for permanent dipole moments in the water. The Debye model has other physical characteristics which make it attractive from an analytical point of view (for details, see [38]).

2.1.2 Lorentz Model

The *Lorentz model* for *electronic* polarization in differential form is represented with the second order equation:

$$\frac{\partial^2\vec{P}}{\partial t^2} + \frac{1}{\tau}\frac{\partial\vec{P}}{\partial t} + \omega_0^2\vec{P} = \epsilon_0\epsilon_d\omega_0^2\vec{E}, \tag{2.6}$$

where $\epsilon_d = \epsilon_s - \epsilon_\infty$ and ω_0 is the resonance frequency of the material.

The Lorentz model is formulated by modeling the atomic structure of the material as a damped vibrating system representing a deformable electron cloud at the atomic level [6]. Applying classical Newtonian laws of motion, we find that the displacement of the outermost shell of the atom satisfies a second-order ordinary differential equation [38].

2.2 Reduction to One Dimension

The electric field is assumed to be polarized to have oscillations in the x-z plane only, as described in [6]. Restricting the problem to one dimension, we can write the electric and magnetic fields, $\vec{E}$ and $\vec{H}$ respectively, as follows

$$\vec{E}(t,\vec{x}) = \hat{i}E(t,z)$$
$$\vec{H}(t,\vec{x}) = \hat{j}H(t,z),$$

so that we are only concerned with the scalar values $E(t,z)$ and $H(t,z)$. In this case Maxwell's equations become

$$\frac{\partial E}{\partial z} = -\mu_0\frac{\partial H}{\partial t} \tag{2.7a}$$
$$-\frac{\partial H}{\partial z} = \frac{\partial D}{\partial t} + J_s. \tag{2.7b}$$

We take the partial derivative of Equation (2.7a) with respect to z, and the partial of Equation (2.7b) with respect to t. Equating the $\frac{\partial^2 H}{\partial z \partial t}$ terms in each, and thus eliminating the magnetic field H, we have

$$E'' = \mu_0 \left(\ddot{D} + \dot{J}_s \right),$$

where $'$ denotes z derivatives and $\dot{}$ denotes time derivatives. Using the constitutive law for he electric flux density given by $D = \epsilon_0 \epsilon_\infty E + P$, we have

$$\mu_0 \epsilon_0 \epsilon_\infty \ddot{E} + \mu_0 \ddot{P} - E'' = -\mu_0 \dot{J}_s \text{ in } \Omega = [a, b]. \tag{2.8}$$

In order to have a finite computational domain, we impose absorbing boundary conditions at $z = a$ and $z = b$, which are modeled as

$$\left[\dot{E} - \mathrm{c} E' \right]_{z=a} = 0, \quad \left[\dot{E} + \mathrm{c} E' \right]_{z=b} = 0, \tag{2.9}$$

where $c = 1/\sqrt{\epsilon_0 \mu_0}$ is the speed of light in vacuum. With these boundary conditions, any incident signal passes out of the computational domain, and does not return. The homogeneous initial conditions in 1D become

$$E(0, z) = 0, \quad P(0, z) = 0, \quad \dot{P}(0, z) = 0, \quad \dot{E}(0, z) = 0. \tag{2.10}$$

3 Numerical Solution

We describe in this section the application of finite elements for the spatial discretization of the model (2.8). The semi-discrete model is then coupled with a polarization model, and the system is discretized in time. The resulting methods are compared in subsequent sections to FDTD methods with respect to stability and dispersion properties.

3.1 Spatial Discretization Using Finite Elements

We apply a finite element method using standard piecewise linear one dimensional basis elements to discretize the model (2.8) in space. Let N be the number of intervals in the uniform discretization of z, and $\Delta z = (b - a)/N$; then the finite element discretization has an order of accuracy of $O(\Delta z^2)$. The resulting system of ordinary differential equations after the spatial discretization is the semi-discrete form

$$\epsilon_\infty \mu_0 \epsilon_0 M \ddot{e} + \mu_0 M \ddot{p} + B \dot{e} + K e = \mu_0 J, \tag{3.1}$$

with either

$$\dot{p} + \lambda p = \epsilon_0 \epsilon_d \lambda e, \text{ (Debye Media)}, \tag{3.2}$$

or

$$\ddot{p} + \lambda \dot{p} + \omega_0^2 p = \epsilon_0 \epsilon_d \omega_0^2 e, \text{ (Lorentz Media)}, \tag{3.3}$$

where $\lambda = \frac{1}{\tau}$. The vectors e and p represent the values of E, and P, respectively at the nodes $z_i = i \Delta z$. The mass matrix M has entries

$$M_{ij} = \langle \phi_i, \phi_j \rangle \ := \int_a^b \phi_i \phi_j dz,$$

where $\{\phi_i\}_{i=0}^N$ are the basis functions. The stability matrix K has entries

$$K_{ij} = \langle \phi_i', \phi_j' \rangle \ := \int_a^b \phi_i' \phi_j' dz.$$

The matrix B results from the boundary conditions where

$$B_{ij} = \frac{1}{c} \left[\phi_i(a)\phi_j(a) - \phi_i(b)\phi_j(b) \right].$$

Finally, J is defined as

$$J_i = -\langle \phi_i, \dot{J}_s \rangle \ := -\int_a^b \dot{J}_s \phi_i dz.$$

For Debye media, we differentiate (3.2) and substitute for $\ddot{p}$ into (3.1) to obtain an equation only dependent explicitly on p, given as

$$\epsilon_\infty M\ddot{e} + (B + \epsilon_d \lambda M)\dot{e} + (c^2 K - \epsilon_d \lambda^2 M)e + \frac{\lambda^2}{\epsilon_0} Mp = \frac{1}{\epsilon_0} J, \tag{3.4a}$$

$$\dot{p} + \lambda p - \epsilon_0 \epsilon_d \lambda e = 0. \tag{3.4b}$$

In the above $c = 1/\sqrt{\epsilon_0 \mu_0}$ is the speed of light in vacuum.

For Lorentz media we substitute (3.3) into (3.1) to obtain

$$\epsilon_\infty M\ddot{e} + B\dot{e} + (c^2 K + \epsilon_d \omega_0^2 M)e - \frac{\omega_0^2}{\epsilon_0} Mp - \frac{\lambda}{\epsilon_0} M\dot{p} = \frac{1}{\epsilon_0} J, \tag{3.5a}$$

$$\ddot{p} + \lambda \dot{p} + \omega_0^2 p = \epsilon_0 \epsilon_d \omega_0^2 e. \tag{3.5b}$$

For linear finite elements in one dimension, the entries of the mass matrix M are

$$M_{ij} = \begin{cases} 2\Delta z/3, & \text{if } 0 < i = j < N, \\ \Delta z/3, & \text{else if } i = j = 0 \text{ or } N, \\ \Delta z/6, & \text{else if } i = j \pm 1. \end{cases} \tag{3.6}$$

The entries of the stiffness matrix can be calculated as

$$K_{ij} = \begin{cases} 2/\Delta z, & \text{if } 0 < i = j < N, \\ 1/\Delta z, & \text{else if } i = j = 0 \text{ or } N, \\ -1/\Delta z, & \text{else if } i = j \pm 1. \end{cases} \tag{3.7}$$

3.2 Time Discretization Using Finite Differences

In order to solve the semi-discrete form of our equations we may convert each coupled second order system of equations into one larger first order system and apply a theta method [23]. As our finite element method is second order in space, if we choose $\theta = \frac{1}{2}$ the discretization is second order in time as well (thus, we have used $\theta = \frac{1}{2}$ throughout). Therefore, for appropriately smooth data and with $\Delta t = O(\Delta z)$, the combined method is second order in time and space. For the system of equations corresponding to the Debye model we consider an additional method of temporal finite difference for comparison. We begin, for completeness, with the simple case of a vacuum.

3.2.1 Free Space (FEM-V)

In vacuum we have $P \equiv 0$, thus, in equation (3.1) we substitute $\ddot{p} = 0$, resulting in

$$\mu_0 \epsilon_0 M \ddot{e} + Ke = 0. \tag{3.8}$$

In the above we have also assumed that $\epsilon_\infty = 1$. Using $\mathrm{c} = 1/\sqrt{\epsilon_0 \mu_0}$, and rewriting (3.8) in first order form in the variables $X = [e^T,\ d^T]^T$, where $d = \dot{e}$, we have

$$\begin{bmatrix} I & 0 \\ 0 & \frac{1}{c^2} M \end{bmatrix} \dot{X} + \begin{bmatrix} 0 & -I \\ K & 0 \end{bmatrix} X = 0. \tag{3.9}$$

Applying a theta scheme to (3.9) we obtain the method **FEM-V**

$$\begin{bmatrix} I & -\theta \Delta t I \\ \theta \Delta t K & \frac{1}{c^2} M \end{bmatrix} X^{n+1} = \begin{bmatrix} I & (1-\theta)\Delta t I \\ -(1-\theta)\Delta t K & \frac{1}{c^2} M \end{bmatrix} X^n. \tag{3.10}$$

3.2.2 Debye Media

In the first method to be considered for the Debye model, we will convert the coupled second order system of equations into one larger first order system and apply a theta method as described above. In the second method, we will solve first for the polarization with a forward differencing scheme using the initial conditions, and then use the polarization solution vector to update a second order central difference scheme for the magnitude of the electric field. We then continue this process iteratively, alternating between solving for p and for e. Both methods are second order in time and space for appropriately smooth data (and with $\Delta t = O(\Delta z)$).

Method 1 (**FEM-D1**): For Debye media we convert (3.4a)-(3.4b) into a first order system of equations in three unknowns, $X = [e^T,\ p^T,\ d^T]^T$, where $d = \dot{e}$, resulting in

$$\bar{M}\dot{X} + \bar{K}X = \bar{J}, \tag{3.11}$$

with

$$\bar{M} = \begin{bmatrix} I & 0 & 0 \\ 0 & I & 0 \\ 0 & 0 & \epsilon_\infty M \end{bmatrix}, \tag{3.12}$$

$$\bar{K} = \begin{bmatrix} 0 & 0 & -I \\ -\epsilon_0 \epsilon_d \lambda & \lambda & 0 \\ (c^2 K - \epsilon_d \lambda^2 M) & \frac{\lambda^2}{\epsilon_0} M & B + \epsilon_d \lambda M \end{bmatrix}, \tag{3.13}$$

and

$$\bar{J} = \begin{bmatrix} 0^T & 0^T & \frac{1}{\epsilon_0} J^T \end{bmatrix}^T. \tag{3.14}$$

We apply a theta-scheme to (3.11) to obtain

$$(\bar{M} + \theta \Delta t \bar{K}) X^{n+1} = (\bar{M} - (1-\theta)\Delta t \bar{K}) X^n + (\theta \bar{J}^{n+1} + (1-\theta)\bar{J}^n). \tag{3.15}$$

For $\theta = 0.5$ the scheme can be written as

$$\left(\bar{M} + \frac{\Delta t}{2}\bar{K}\right) X^{n+1} = \left(\bar{M} - \frac{\Delta t}{2}\bar{K}\right) X^n + \frac{1}{2}\left(\bar{J}^{n+1} + \bar{J}^n\right). \tag{3.16}$$

where, $\bar{J}^n = \bar{J}(n\Delta t)$ and $X^n = X(n\Delta t)$.

As we are assuming a fixed time step Δt, the matrix to be inverted does not change over time. Therefore, in our implementation we solve for the LU factorization at the beginning and use back substitution at each time step. Since the matrices $\bar{M}$ and $\bar{K}$ are sparse, we employ the sparse matrix package UMFPACK [14]. For problems where the number of time steps is small compared with the number of nodes, it may be more efficient to use an iterative solver with the previous solution vector as the initial iterate. The choice of linear solver does not affect the stability or dispersion properties of the method, which are the focal points of this report.

Method 2 (**FEM-D2**): In our second method we use a second order central difference scheme to solve (3.4a). Our approach is to first solve for p using a θ-method, and then use that approximation to solve for e at the next time step. Thus, our finite difference approximation for (3.4b) is

$$p^{n+1} = p^n - \Delta t\lambda p^{n+\theta} + \Delta t\lambda\epsilon_d e^{n+\theta} \tag{3.17}$$

where $v^{n+\theta} = \theta v^{n+1} + (1-\theta)v^n$, for $v = e$ or $v = p$. This implies

$$p^{n+1} = p^n + \frac{\lambda\Delta t}{1 + \lambda\Delta t\theta}(\epsilon_d e^{n+\theta} - p_n). \tag{3.18}$$

Once we have p^{n+1} we can solve for e^{n+2}. Applying second order central difference with averaging to (3.4a) gives

$$\begin{aligned}&\frac{1}{\Delta t^2}\epsilon_\infty M(e^{n+2} - 2e^{n+1} + e^n) + \frac{1}{2\Delta t}(B + \epsilon_d\lambda M)(e^{n+2} - e^n)\\ &+ \frac{1}{4}(c^2K - \epsilon_d\lambda^2 M)(e^{n+2} + 2e^{n+1} + e^n) = \frac{1}{\epsilon_0}J^{n+1} - \frac{\lambda^2}{\epsilon_0}M\bar{p}^{n+1}.\end{aligned} \tag{3.19}$$

Defining $h_\tau = \lambda\Delta t$ and solving for the e^{n+2} term we have

$$\begin{aligned}&\left[\left(\epsilon_\infty + \frac{\epsilon_d h_\tau}{2} - \frac{\epsilon_d h_\tau^2}{4}\right)M + \frac{1}{2}\Delta t B\right]e^{n+2} = \left[(2\epsilon_\infty + \frac{\epsilon_d h_\tau^2}{2})M - \frac{c^2\Delta t^2}{2}K\right]e^{n+1}\\ &- \left[(\epsilon_\infty - \frac{\epsilon_d h_\tau}{2} - \frac{\epsilon_d h_\tau^2}{4})M + \frac{c^2\Delta t^2}{4}K + \frac{1}{2}\Delta t B\right]e^n + \frac{\Delta t^2}{\epsilon_0}J^{n+1} - \frac{h_\tau^2}{\epsilon_0}Mp^{n+1}\end{aligned} \tag{3.20}$$

or equivalently,

$$A_1 e^{n+2} = A_2 e^{n+1} + A_3 e^n + \frac{\Delta t^2}{\epsilon_0}J^{n+1} - \frac{h_\tau^2}{\epsilon_0}Mp^{n+1}. \tag{3.21}$$

Note that in this case A_1 is tridiagonal and the matrix is the same for each time step, so we may store the Crout LU factorization and use back substitution to solve the

system at each time step. For tridiagonal matrices the factorization and the back substitution are both order $O(N)$ [23].

Again, for $\theta = \frac{1}{2}$, (3.18) will be second order in time if the corresponding solution is C^3 in time. Equation (3.21) is also second order in time assuming an exact solution for P, and that E has four continuous time derivatives (for the second order difference approximation). The truncation error for this approximation is

$$T(t_n) = \Delta t^2 \left(\frac{1}{12} E^{(4)} + \frac{1}{6} E^{(3)} + \frac{1}{4} E^{(2)} \right).$$

Therefore, since the semi-discrete form is $O(h^2)$, this approximation method overall is $O(h^2)$ when $\Delta t = O(h)$.

3.2.3 Lorentz Media (FEM-L)

For Lorentz media we consider only the approach of converting (3.5a)-(3.5b) into a first order system of equations, which with a theta method for the temporal discretization, we will refer to as the **FEM-L** method. The linear ODE system is in terms of three unknowns, $X = [e^T,\ p^T,\ d^T,\ q^T]^T$, where $d = \dot{e}, q = \dot{p}$, and can be written as

$$\bar{M}\dot{X} + \bar{K}X = \bar{J}, \tag{3.22}$$

with

$$\bar{M} = \begin{bmatrix} I & 0 & 0 & 0 \\ 0 & I & 0 & 0 \\ 0 & 0 & \epsilon_\infty M & 0 \\ 0 & 0 & 0 & I \end{bmatrix}, \tag{3.23}$$

$$\bar{K} = \begin{bmatrix} 0 & 0 & -I & 0 \\ 0 & 0 & 0 & -I \\ (c^2 K + \epsilon_d \omega_0^2 M) & -\frac{\omega_0^2}{\epsilon_0} M & B & -\frac{\lambda}{\epsilon_0} M \\ -\epsilon_0 \epsilon_d \omega_0^2 & \omega_0^2 & 0 & \lambda \end{bmatrix}, \tag{3.24}$$

and

$$\bar{J} = \begin{bmatrix} 0^T & 0^T & \frac{1}{\epsilon_0} J^T & 0^T \end{bmatrix}^T. \tag{3.25}$$

As stated above, we apply a theta-scheme to $\bar{M}\dot{X} + \bar{K}X = \bar{J}$ to obtain

$$(\bar{M} + \theta \Delta t \bar{K}) X^{n+1} = (\bar{M} - (1-\theta)\Delta t \bar{K}) X^n + (\theta \bar{J}^{n+1} + (1-\theta)\bar{J}^n), \tag{3.26}$$

For $\theta = 0.5$ the scheme can be written as

$$\left(\bar{M} + \frac{\Delta t}{2} \bar{K} \right) X^{n+1} = \left(\bar{M} - \frac{\Delta t}{2} \bar{K} \right) X^n + \frac{1}{2} \left(\bar{J}^{n+1} + \bar{J}^n \right). \tag{3.27}$$

where, $\bar{J}^n = \bar{J}(n\Delta t)$ and $X^n = X(n\Delta t)$.

Again we are assuming a fixed Δt, therefore, in implementation, we solve for the LU factorization at the beginning and use back substitution at each time step.

4 Stability Analysis

Fourier analysis is an important tool in the study of stability of finite difference and finite element schemes. The Fourier transform of a function gives an alternative representation of the function, and one can infer certain properties of a function from its Fourier transform. The Fourier inversion formula represents a function as a superposition of waves $\mathrm{e}^{i\omega z}$ with different amplitudes that are given by the Fourier transform. Under the Fourier transform the operation of differentiation is converted into the operation of multiplication by $\mathrm{i}\omega$.

An important application of Fourier analysis is the von Neumann analysis of stability of difference schemes. With the use of Fourier analysis we can give necessary and sufficient conditions for the stability of these schemes. For a difference scheme, advancing the solution of the scheme by one time step is equivalent to multiplying the Fourier transform of the solution by an *amplification factor*. The amplification factor is so called because its magnitude is the amount that the amplitude of each frequency in the solution, given by the Fourier transform of the solution at time step n, is amplified in advancing the solution to time step $n+1$. All the information of a scheme is contained in its amplification factor. In particular, the stability and accuracy of schemes can be determined from the amplification factor. Using Fourier analysis on the scheme to calculate the amplification factor ζ is equivalent to replacing discrete values of any unknown field vector v_m^n, at time $t = n\Delta t$ and spatial position $z = m\Delta z$, in the scheme by $\zeta^n e^{\mathrm{i}m\theta}$ for each value of n and m. The resulting equation is a polynomial in ζ and is called the *stability polynomial* or the *characteristic polynomial* for the scheme. The stability polynomial usually depends on the discretization parameters, such as the time step and the mesh step size as well as the medium parameters. The roots of this polynomial can be obtained and will determine the stability of the scheme. Since the roots of the polynomial are the amplification factors of the scheme, the scheme will be stable if the amplitude of the roots is less than or equal to 1.

We follow here the approach used in [29] for the FDTD in order to derive stability results for the finite element schemes described above. We will compare our results with those obtained in [29] for FDTD schemes treating both Debye and Lorentz models. Namely, for Debye, we consider the scheme in [19] (which we will refer to as JHT-D) and the scheme in [21] (KF-D). Regarding the Lorentz model for polarization, we compare results with JHT-L [19] and KF-L [20].

Note that, since the boundary conditions do not affect the stability and dispersion properties of the scheme in the interior of the domain, we neglect the effects of boundary conditions, i.e., we take $B = 0$ in (3.1), in our analysis. Further, as the stability and dispersion properties of the scheme are also independent of the source J_s, we take $J = 0$ in (3.1) without loss of generality.

4.1 Free Space

We note the following identities associated with the application of the mass and the stiffness matrices on vectors $\phi_j^n = \tilde{\phi}\zeta^n \mathrm{e}^{i(kj\Delta z)}$

1. For the mass matrix M we have

$$\begin{aligned} M\phi_j^n &= \frac{\Delta z}{6}\phi_{j-1}^n + \frac{2\Delta z}{3}\phi_j^n + \frac{\Delta z}{6}\phi_{j+1}^n \\ &= \left(\mathrm{e}^{-ik\Delta z} + 4 + \mathrm{e}^{ik\Delta z}\right)\frac{\Delta z}{6}\phi_j^n \\ &= (3 - 2\sin^2(k\Delta z/2))\frac{\Delta z}{3}\phi_j^n \end{aligned} \tag{4.1}$$

2. For the stiffness matrix K we have

$$\begin{aligned} K\phi_j^n &= -\frac{1}{\Delta z}\phi_{j-1}^n + \frac{2}{\Delta z}\phi_j^n - \frac{1}{\Delta z}\phi_{j+1}^n \\ &= \left(\mathrm{e}^{-ik\Delta z} - 2 + \mathrm{e}^{ik\Delta z}\right)\frac{-1}{\Delta z}\phi_j^n \\ &= \frac{4}{\Delta z}\sin^2(k\Delta z/2))\phi_j^n. \end{aligned} \tag{4.2}$$

We also define two quantities

$$\kappa = 3 - 2\sin^2\left(\frac{k\Delta z}{2}\right), \tag{4.3a}$$

$$\eta = 3\nu^2\sin^2\left(\frac{k\Delta z}{2}\right), \tag{4.3b}$$

where the *Courant number* is

$$\nu = \frac{\mathrm{c}\Delta t}{\Delta z},\ (\epsilon_\infty = 1). \tag{4.4}$$

In a general dispersive material $\nu = \frac{\mathrm{c}\Delta t}{\sqrt{\epsilon_\infty}\Delta z}$. In air $\epsilon_\infty = 1$. To determine the stability criterion for the finite element scheme in vacuum, FEM-V, we now substitute

$$X_j^n = \begin{bmatrix} e_j^n \\ d_j^n \end{bmatrix} = \begin{bmatrix} \tilde{e} \\ \tilde{d} \end{bmatrix}\zeta^n \mathrm{e}^{\mathrm{i}(kj\Delta z)}, \tag{4.5}$$

into the discrete equations (3.10) with $\theta = 1/2$. Here k is the wave number, Using the identities (4.1) and (4.2) we obtain a homogeneous linear system of the form

$$\mathcal{A}\tilde{\mathcal{X}} = 0, \tag{4.6}$$

with

$$\mathcal{A} = \begin{bmatrix} \zeta - 1 & -\frac{\Delta t}{2}(\zeta + 1) \\ \dfrac{2\Delta t}{\Delta z}\sin^2\left(\dfrac{k\Delta z}{2}\right)(\zeta + 1) & \dfrac{\Delta z}{3c^2}\left(3 - 2\sin^2\left(\dfrac{k\Delta z}{2}\right)\right)(\zeta - 1) \end{bmatrix} \tag{4.7}$$

and

$$\tilde{\mathcal{X}} = \begin{bmatrix} \tilde{e}^T & \tilde{d}^T \end{bmatrix}^T. \tag{4.8}$$

By setting the determinant of $\mathcal{A}$ to be zero, we obtain the stability polynomial

$$\zeta^2 - 2\zeta\left(\frac{\kappa^2 - \eta^2}{\kappa^2 + \eta^2}\right) + 1 = 0, \tag{4.9}$$

From (4.9) we can show that $|\zeta| = 1$ always, regardless of the medium parameters. This implies that the finite element scheme with the theta method ($\theta = 1/2$) in *free space*, FEM-V, is *unconditionally stable* as well as *non-dissipative*.

4.2 Debye Media

To determine the stability conditions for the finite element scheme FEM-D1 described in Section 3.2.2 for Debye media we substitute

$$X_j^n = \begin{bmatrix} e_j^n \\ p_j^n \\ d_j^n \end{bmatrix} = \begin{bmatrix} \tilde{e} \\ \tilde{p} \\ \tilde{d} \end{bmatrix} \zeta^n \mathrm{e}^{\mathrm{i}kj\Delta z}, \tag{4.10}$$

in the discrete equations (3.16) (with $J = 0$). As in the case of free space, we obtain a homogeneous system of the type $\mathcal{A}\tilde{\mathcal{X}} = 0$. We then set $\det(\mathcal{A}) = 0$ to obtain the stability polynomial

$$a_3\zeta^3 + a_2\zeta^2 + a_1\zeta + a_0 = 0, \tag{4.11}$$

where the coefficients of the stability polynomial are given by

$$a_3 = \eta^2(h_\tau + 2) + \kappa^2(h_\tau\epsilon_s + 2\epsilon_\infty), \tag{4.12}$$

$$a_2 = \eta^2(3h_\tau + 2) - \kappa^2(h_\tau\epsilon_s + 6\epsilon_\infty), \tag{4.13}$$

$$a_1 = \eta^2(3h_\tau - 2) - \kappa^2(h_\tau\epsilon_s - 6\epsilon_\infty), \tag{4.14}$$

$$a_0 = \eta^2(h_\tau - 2) + \kappa^2(h_\tau\epsilon_s - 2\epsilon_\infty), \tag{4.15}$$

where η, and κ are as defined in (4.3b), and (4.3a), respectively, and $h_\tau = \Delta t/\tau$.

To determine the stability polynomial for the finite element scheme FEM-D2 described in Section (3.2.2), we substitute (4.10) in the discrete equations (3.20). Following the procedure discussed above we obtain the stability polynomial

$$b_3\zeta^3 + b_2\zeta^2 + b_1\zeta + b_0 = 0, \tag{4.16}$$

with coefficients

$$b_3 = \eta^2(h_\tau + 2) + \kappa^2(h_\tau\epsilon_s + 2\epsilon_\infty) - \frac{\kappa^2 h_\tau^3\epsilon_d}{4}, \tag{4.17}$$

$$b_2 = \eta^2(3h_\tau + 2) - \kappa^2(h_\tau\epsilon_s + 6\epsilon_\infty) + \frac{\kappa^2 h_\tau^3\epsilon_d}{4}, \tag{4.18}$$

$$b_1 = \eta^2(3h_\tau - 2) - \kappa^2(h_\tau\epsilon_s - 6\epsilon_\infty) + \frac{\kappa^2 h_\tau^3\epsilon_d}{4}, \tag{4.19}$$

$$b_0 = \eta^2(h_\tau - 2) + \kappa^2(h_\tau\epsilon_s - 2\epsilon_\infty) - \frac{\kappa^2 h_\tau^3\epsilon_d}{4}, \tag{4.20}$$

If we neglect terms involving h_τ^3, the stability polynomial of FEM-D2 is the same as in FEM-D1. Thus for small values of h_τ, the two methods have the same stability properties. For example, in [5] a plot of $\max|\zeta|$ versus $k\Delta z$ is given for $h_\tau = 0.1$ and $h_\tau = 0.3$ for the finite element schemes FEM-D1 and FEM-D2, with $\nu = 1$. From this plot one can see a slight difference in the two schemes when $h_\tau = 0.3$. However, for $h_\tau = 0.1$ the two schemes are indistinguishable. Therefore, in the rest of this section we will consider only FEM-D1, and may refer to it as *the finite element scheme* for the Debye model. Similarly, it was shown in [29] that the stability properties for the two FDTD methods JHT-D [19] and

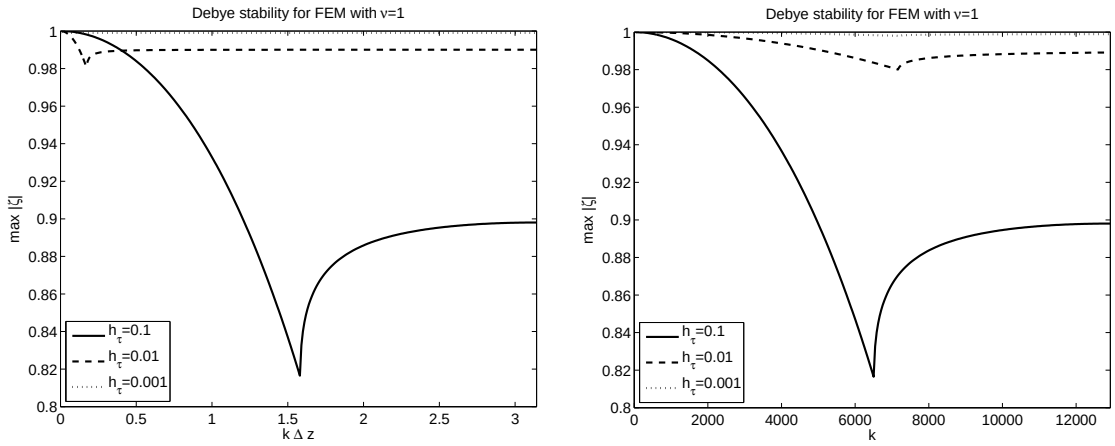

Figure 1: Plot on left (right) is of $\max|\zeta|$ versus $k\Delta z$ (resp., k) for $h_\tau \in \{0.1, 0.01, 0.001\}$ for the FEM-D1 scheme, with $\nu = 1$.

KF-D [21] are identical. Therefore, in the remainder of this section we will consider only JHT-D, and may refer to it as *the finite difference scheme* for the Debye model. We will compare stability properties of the finite element scheme FEM-D1 with those of the finite difference scheme JHT-D, understanding that the corresponding conclusions drawn therein apply equally to the methods FEM-D2 and KF-D.

In the left plot of Figure 1 we graph the absolute value of the largest root of (4.11), as a function of $k\Delta z$, for the finite element scheme FEM-D1 using $\nu = 1$. In Figure 2 we plot the the absolute value of the largest root of the stability polynomial of the finite difference scheme JHT [19], with $\nu = 1$ as a function of $k\Delta z$. In each figure, the right plot depicts the same quantity, but versus the wave number k.

To generate these plots we assumed the following values of the physical parameters, as considered in [6] (note that these are appropriate constants for modeling water)

$$\epsilon_\infty = 1, \tag{4.21a}$$

$$\epsilon_s = 78.2, \tag{4.21b}$$

$$\tau = 8.1 \times 10^{-12} \text{ sec.} \tag{4.21c}$$

These values will be used throughout for any numerical examples involving the Debye polarization model. The time step Δt is determined by the choice of h_τ and the physical parameter τ. These plots show varying values of h_τ from 0.1 to 0.001. From the plots we can see that the dissipation of the numerical schemes can be reduced by decreasing h_τ. For stability and least dissipation, $h_\tau = 0.001$ is recommended. For the finite element scheme FEM-D1, increasing ν from 1 to 16 does not appear to change the stability behavior of the scheme. This suggests the *unconditional stability* of *the finite element scheme*. However, *the finite difference scheme is conditionally stable* and has the stability criteria $\nu \leq 1$. The stability criteria for the finite difference scheme have been derived in [29, 11].

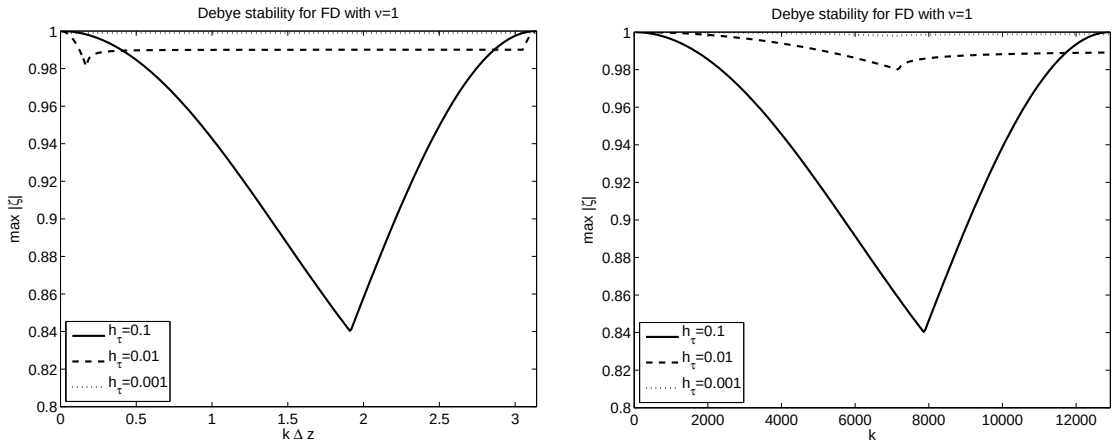

Figure 2: Plot on left (right) is of $\max|\zeta|$ versus $k\Delta z$ (resp., k) for $h_\tau \in \{0.1, 0.01, 0.001\}$ for the JHT-D scheme, with $\nu = 1$.

4.3 Lorentz Media

To determine the stability conditions for the finite element method applied to the Lorentz media, FEM-L, we substitute

$$X_j^n = \begin{bmatrix} e_j^n \\ p_j^n \\ d_j^n \\ q_j^n \end{bmatrix} = \begin{bmatrix} \tilde{e} \\ \tilde{p} \\ \tilde{d} \\ \tilde{q} \end{bmatrix} \zeta^n \mathrm{e}^{\mathrm{i}kj\Delta z}, \tag{4.22}$$

in the discrete equations (3.27). As in the case of free space, we obtain a homogeneous system of the type $\mathcal{A}\tilde{\mathcal{X}} = 0$. We then set $\det(\mathcal{A}) = 0$ to obtain the stability polynomial

$$a_4\zeta^4 + a_3\zeta^3 + a_2\zeta^2 + a_1\zeta + a_0 = 0, \tag{4.23}$$

where the coefficients of the stability polynomial are given by

$$a_4 = \eta^2(2\pi^2 h_0^2 + h_\tau + 2) + \kappa^2(2\pi^2 h_0^2\epsilon_s + h_\tau\epsilon_\infty + 2\epsilon_\infty) \tag{4.24}$$
$$a_3 = \eta^2(8\pi^2 h_0^2 + 2h_\tau) - \kappa^2\epsilon_\infty(8 + 2h_\tau) \tag{4.25}$$
$$a_2 = \eta^2(12\pi^2 h_0^2 - 4) - \kappa^2(4\pi^2 h_0^2\epsilon_s - 12\epsilon_\infty) \tag{4.26}$$
$$a_1 = \eta^2(8\pi^2 h_0^2 - 2h_\tau) - \kappa^2\epsilon_\infty(8 - 2h_\tau) \tag{4.27}$$
$$a_0 = \eta^2(2\pi^2 h_0^2 - h_\tau + 2) - \kappa^2(2\pi^2 h_0^2\epsilon_s - h_\tau\epsilon_\infty + 2\epsilon_\infty), \tag{4.28}$$

where η, and κ are as defined in (4.3b), and (4.3a), respectively, $h_\tau = \Delta t/\tau$, and $h_0 = \Delta t/T_0$, where $T_0 = 2\pi/\omega_0$.

We seek to compare the stability properties of FEM-L to the finite difference schemes JHT-L [19] and KF-L [20]. We plot the absolute value of the largest root of (4.23) for $\nu = 1$ versus $k\Delta z$ for the FEM-L in Figure 3 (left), and for the schemes JHT-L and KF-L, we plot

the corresponding functions on the left in Figures 4 and 5, respectively. In each figure, the right plot depicts the same function, but versus the wave number k.

To generate these plots we assumed the following values for physical parameters, as considered in [6]:

$$\epsilon_\infty = 1, \tag{4.29a}$$

$$\epsilon_s = 2.25, \tag{4.29b}$$

$$\tau = 1.786 \times 10^{-16} \text{ sec}, \tag{4.29c}$$

$$\omega_0 = 4 \times 10^{16} \text{ rad/sec}. \tag{4.29d}$$

These values will be used throughout in any numerical examples involving the Lorentz polarization model.

For the Lorentz medium, all time scales must be properly resolved, therefore the time step Δt is determined by the choice of either h_τ or h_0, whichever is most restrictive. For the current parameter values, $T_0 < \tau$, thus h_0 is used. The plots show varying values of h_0 from 0.1 to 0.001. From the plots we can see that the dissipation of the numerical schemes can be reduced by decreasing h_0. For stability and least dissipation, $h_0 = 0.01$ is recommended.

As in the case of the finite element method for Debye media, FEM-D1, we see that increasing ν from 1 to 16 does not affect the stability properties of the finite element scheme for Lorentz media, FEM-L. This suggests the *unconditional stability* of the *finite element method* for Lorentz media. However, again *the finite difference scheme is conditionally stable* with the criteria $\nu \leq 1$. The stability criteria for the finite difference scheme for Lorentz media have been derived in [29, 11].

5 Analysis of Dispersion and Phase Error

The numerical models presented admit plane wave solutions of the form $\mathrm{e}^{\mathrm{i}(\omega t - \vec{k}\cdot\vec{x})}$ for which the speed of propagation, governed by the wave number $\vec{k}$, erroneously depends on the frequency ω. The resulting error in the solution, which is an artifact of discretization, is termed as numerical dispersion. For time-harmonic waves, numerical dispersion results in the creation of a numerical phase velocity error, or *phase error*, in the solution. This is due to the incorrect modeling of the sinusoidal behavior of the propagating wave; for example, the piecewise polynomial approximation of a finite element method does not exactly match a sine or cosine function. Dispersion is present in numerical approximation methods such as finite difference/finite element methods even in the absence of any dispersion in the actual media. As waves propagate over long distances numerical dispersion errors accumulate in the solution and may cause it to completely deviate from the correct solution.

5.0.1 Free Space

Substituting a solution of the form

$$e(t, z) = \mathrm{e}^{\mathrm{i}(kz - \omega t)}$$

into equation (2.8), we obtain the dispersion relation of the continuous model in free space

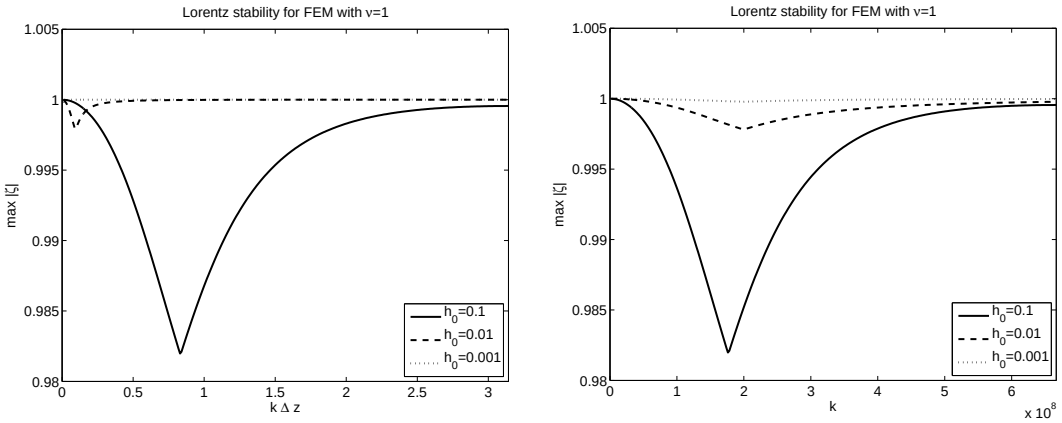

Figure 3: Plot on left (right) is of $\max|\zeta|$ versus $k\Delta z$ (resp., k) for $h_\tau \in \{0.1, 0.01, 0.001\}$ for the FEM-L scheme, with $\nu = 1$.

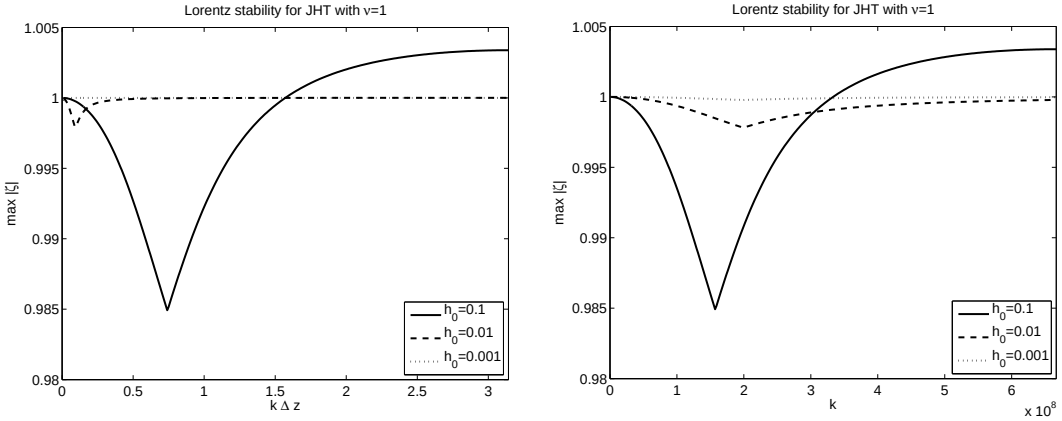

Figure 4: Plot on left (right) is of $\max|\zeta|$ versus $k\Delta z$ (resp., k) for $h_\tau \in \{0.1, 0.01, 0.001\}$ for the JHT-L scheme, with $\nu = 1$.

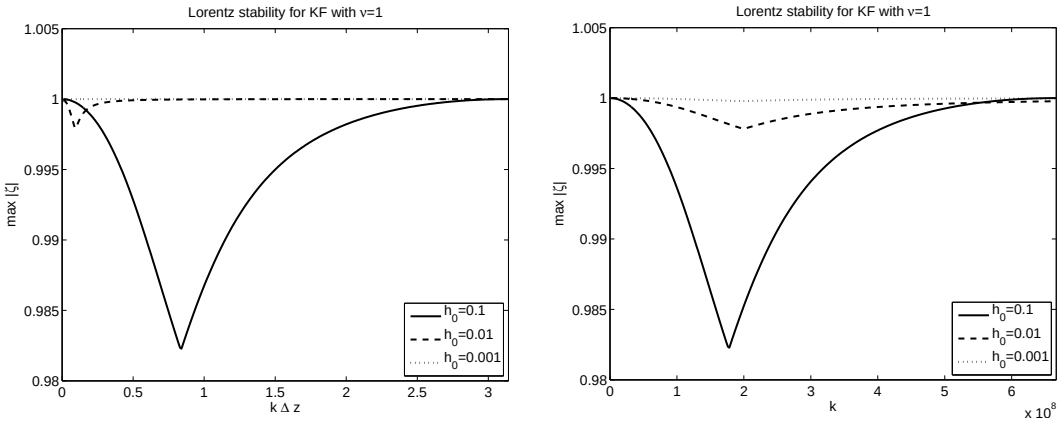

Figure 5: Plot on left (right) is of $\max|\zeta|$ versus $k\Delta z$ (resp., k) for $h_\tau \in \{0.1, 0.01, 0.001\}$ for the KF-L scheme, with $\nu = 1$.

given by

$$k_{\mathrm{EX}}^{\mathrm{V}}(\omega) = \frac{\omega}{\mathrm{c}}, \tag{5.1}$$

where $k_{\mathrm{EX}}^{\mathrm{V}}$ denotes the wavenumber in free space (where V in the superscript denotes "vacuum") for the exact equations (EX in the subscript denotes "exact"). To determine the dispersion relation for the discretized model using the finite element method FEM-V, we substitute

$$X_j^n = \begin{bmatrix} e_j^n \\ d_j^n \end{bmatrix} = \begin{bmatrix} \tilde{e} \\ \tilde{d} \end{bmatrix} \mathrm{e}^{\mathrm{i}(k_\Delta j \Delta z - \omega n \Delta t)}, \tag{5.2}$$

where k_Δ is the numerical wave number, into the discrete equation (3.10). Using the identities (4.1), (4.2) as well as the following two trigonometric identities

$$\mathrm{e}^{-\mathrm{i}\omega\Delta t/2} + \mathrm{e}^{\mathrm{i}\omega\Delta t/2} = 2\cos(\omega\Delta t/2), \tag{5.3a}$$

$$\mathrm{e}^{-\mathrm{i}\omega\Delta t/2} - \mathrm{e}^{\mathrm{i}\omega\Delta t/2} = -2\mathrm{i}\sin(\omega\Delta t/2). \tag{5.3b}$$

we obtain the linear system

$$\mathcal{A}\tilde{\mathcal{X}} = 0, \tag{5.4}$$

with

$$\mathcal{A} = \begin{bmatrix} 2\mathrm{i}\sin\left(\frac{\omega\Delta t}{2}\right) & \Delta t\cos\left(\frac{\omega\Delta t}{2}\right) \\ \frac{4\Delta t}{\Delta z}\sin^2\left(\frac{k_\Delta \Delta z}{2}\right)\cos\left(\frac{\omega\Delta t}{2}\right) & -\frac{\Delta z}{3c^2}\left(3 - 2\sin^2\left(\frac{k_\Delta\Delta z}{2}\right)\right)2\mathrm{i}\sin\left(\frac{\omega\Delta t}{2}\right) \end{bmatrix}$$

and

$$\tilde{\mathcal{X}} = \begin{bmatrix} \tilde{e}^T & \tilde{d}^T \end{bmatrix}^T. \tag{5.5}$$

Setting the determinant of $\mathcal{A} = 0$ we obtain a relation between k_Δ and ω, which is the numerical dispersion relation for the finite element scheme in free space, FEM-V. This relation is

$$\sin^2(k_\Delta \Delta z/2) = \left(\frac{2}{3} + \frac{\nu^2\cos^2(\omega\Delta t/2)}{\sin^2(\omega\Delta t/2)}\right)^{-1}. \tag{5.6}$$

Solving for k_Δ in the above we obtain

$$k_\Delta = k_{\mathrm{FE}}^{\mathrm{V}}(\omega) = \frac{2}{\Delta z}\sin^{-1}\left(\frac{1}{\sqrt{\frac{2}{3} + \frac{\nu^2\cos^2(\omega\Delta t/2)}{\sin^2(\omega\Delta t/2)}}}\right). \tag{5.7}$$

The dispersion relation for the FDTD scheme [36] is given to be

$$\sin(k_\Delta \Delta z/2) = \frac{\sin(\omega\Delta t/2)}{\nu}, \tag{5.8}$$

which implies that

$$k_\Delta = k_{\mathrm{FD}}^{\mathrm{V}}(\omega) = \frac{2}{\Delta z}\sin^{-1}\left[\frac{\sin(\omega\Delta t/2)}{\nu}\right]. \tag{5.9}$$

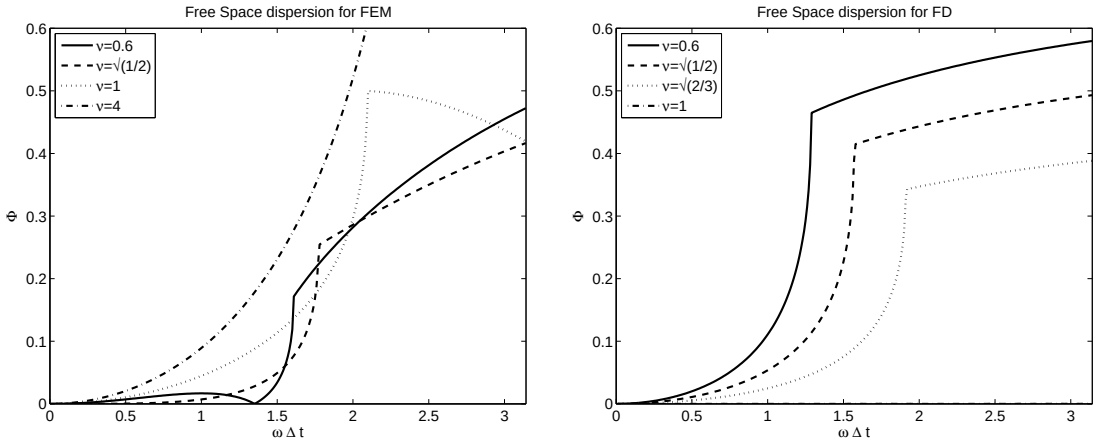

Figure 6: Plot of the phase error Φ versus $\omega\Delta t$ for FEM-V with $\nu \in \{\sqrt{1/2}, 1, 4, 16\}$ (left), and FDTD in freespace with $\nu = \{1, \sqrt{2/3}, \sqrt{1/2}, .6\}$ (right). For $\nu = 1$ FDTD has zero dispersion.

We will define the phase error for a given method as

$$\Phi(\omega\Delta t) = \left| \frac{k_{\mathrm{EX}}(\omega\Delta t) - k_{\Delta}(\omega\Delta t)}{k_{\mathrm{EX}}(\omega\Delta t)} \right|, \tag{5.10}$$

where for FEM-V we have $k_\Delta = k^{\mathrm{V}}_{\mathrm{FE}}$ as defined in (5.7), and for the FDTD scheme we have $k_\Delta = k^{\mathrm{V}}_{\mathrm{FD}}$ as defined in (5.9).

In Figure 6 we plot the phase error in a vacuum for the FEM-V scheme with the theta method using $\nu \in \{\sqrt{1/2}, 1, 4, 16\}$ (left) and for the FDTD scheme using $\nu \in \{0.6, \sqrt{1/2}, \sqrt{2/3}, 1\}$ (right).

To see why $\nu \approx .7$ has the least dispersion for FEM-V and why $\nu \approx 1$ has the least dispersion for the FDTD scheme, it is helpful to plot the relations in equations (5.6) and (5.8) versus the continuous model values. We define

$$\gamma^2_{\mathrm{EX}} := \sin^2\left(\frac{\omega dt}{2\nu}\right) \tag{5.11}$$

where we have substituted $k^{\mathrm{V}}_{\mathrm{EX}}\Delta z = \nu\omega\Delta t$. We similarly define $\gamma^2_{\mathrm{FE}} = \sin^2(k^{\mathrm{V}}_{\mathrm{FE}}\Delta z/2)$ and $\gamma^2_{FD} = \sin^2(k^{\mathrm{V}}_{\mathrm{FD}}\Delta z/2)$ using the definitions in (5.7) and (5.9), respectively. Figure 7 displays plots each of these $\gamma^2(\omega\Delta t)$ functions for various values of ν. For the continuous model (left plot), ν has the effect of moving the location of the maximum value, $\gamma^2 = 1$. For the finite difference case (right plot) the location of the maximum does not change, although the value of the maximum does. For $\nu = 1$ the curve coincides exactly with the continuous case. For the finite element method (middle plot) the location of the maximum does not change, nor does the value. However, as this value is fixed at 1.5, it will *never* coincide exactly with the continuous case for any value of ν.

To determine the *best* value of ν for the finite element method, we first note that γ^2_{EX}

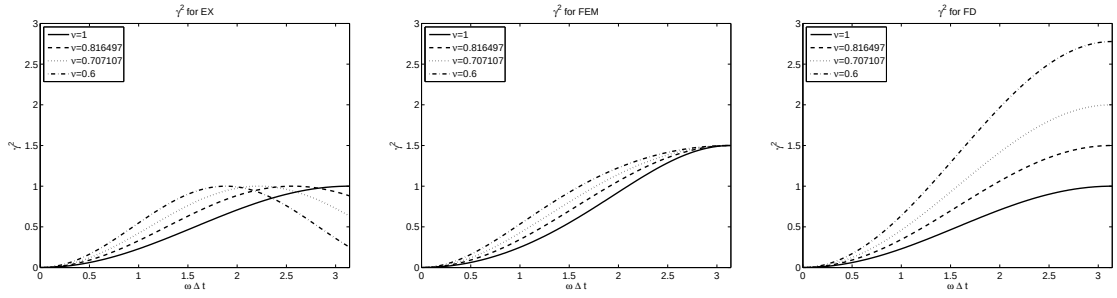

Figure 7: Plot of the γ^2 versus $\omega\Delta t$ for the continuous model, the finite elment scheme, and the finite difference scheme (left to right).

can be expanded as

$$1/4\,\frac{\omega^2 \Delta t^2}{\nu^2} - 1/48\,\frac{\omega^4 \Delta t^4}{\nu^4} + \frac{1}{1440}\,\frac{\omega^6 \Delta t^6}{\nu^6} + O\left(\omega^8 \Delta t^8\right). \tag{5.12}$$

As both the expansions of γ_{FD} and γ_{FE} match up to the second order coefficient, it is the fourth order Taylor coefficient that determines how well the discretization method matches the continuous model. For the finite difference method we have

$$c_4^{\mathrm{FD}} = -1/48\,\nu^{-2}, \tag{5.13}$$

whereas for the finite element method we have

$$c_4^{\mathrm{FE}} = 1/24\,\frac{-1+\nu^2}{\nu^4}. \tag{5.14}$$

For $\nu = 1$, $c_4^{\mathrm{FD}} = c_4^{\mathrm{EX}} = 1/48$, but $c_4^{\mathrm{FE}} = 0$. If we solve $(c_4^{\mathrm{EX}} - c_4^{\mathrm{FE}})(\nu) = 0$ we find that $\nu = \sqrt{1/2}$ is the value for which the finite element method most closely matches the continuous model. It can be shown that for $\nu = \sqrt{2/3}$ the FEM-V scheme is similar to the FDTD scheme (see [5] for details). Further, for $\nu = \sqrt{1/2}$, FEM-V has phase velocity (propagation speed scaled by $\frac{1}{\mathrm{c}}$) closest to one–see [5]. For $\nu = 1$ FDTD always has velocity one.

5.0.2 Debye Media

The dispersion relation for the continuous Debye model is given by

$$k_{\mathrm{EX}}^{\mathrm{D}}(\omega) = \frac{\omega}{\mathrm{c}}\sqrt{\epsilon_r^{\mathrm{D}}(\omega)}. \tag{5.15}$$

where

$$\epsilon_r^{\mathrm{D}}(\omega) = \frac{\epsilon_s \lambda - \mathrm{i}\omega}{\lambda - \mathrm{i}\omega}, \tag{5.16}$$

is the relative complex permittivity of the Debye medium, $\lambda = 1/\tau$. To determine the numerical dispersion relation for the finite element method FEM-D1, described in Section

3.2.2, we substitute

$$X_j^n = \begin{bmatrix} e_j^n \\ p_j^n \\ d_j^n \end{bmatrix} = \begin{bmatrix} \tilde{e} \\ \tilde{p} \\ \tilde{d} \end{bmatrix} \mathrm{e}^{\mathrm{i}(k_\Delta j\Delta z - \omega n\Delta t)} \tag{5.17}$$

in the discrete equations (3.16) (with $J = 0$). We assume again that $\epsilon_\infty = 1$. As in the case of free space, we obtain a homogeneous system of the type $\mathcal{A}\tilde{\mathcal{X}} = 0$. We then set $\det(\mathcal{A}) = 0$ to obtain a relation between the numerical wavenumber k_Δ and the frequency ω. Solving for k_Δ in this relation, and writing in a form comparable to (5.15), we obtain the numerical dispersion relation for the FEM-D1 scheme to be

$$k_\Delta = k_{\mathrm{FE}}^{\mathrm{D}}(\omega) = \frac{2}{\Delta z}\sin^{-1}\left[\frac{\omega_\Delta}{c}\frac{\Delta z}{2}\sqrt{\epsilon_{r,\mathrm{FE}}^{\mathrm{D}}}\right], \tag{5.18}$$

with the discrete relative complex permittivity given by

$$\epsilon_{r,\mathrm{FE}}^{\mathrm{D}} = \frac{\epsilon_{s,\Delta}\lambda_\Delta - \mathrm{i}\omega_\Delta}{\lambda_\Delta - \mathrm{i}\omega_\Delta}, \tag{5.19}$$

where the discrete medium parameters are

$$\epsilon_{s,\Delta} = \frac{\epsilon_s}{\alpha^2\beta^2} \tag{5.20}$$

$$\lambda_\Delta = \lambda\cos(\omega\Delta t/2)\beta^2\alpha^3 \tag{5.21}$$

$$\omega_\Delta = \omega s_\omega \alpha \tag{5.22}$$

and

$$s_\omega = \frac{\sin(\omega\Delta t/2)}{\omega\Delta t/2} \tag{5.23}$$

$$\alpha = \left(\frac{2\sin^2(\omega\Delta t/2)}{3\nu^2} + \cos^2(\omega\Delta t/2)\right)^{-1/2} \tag{5.24}$$

$$\beta = \left(\frac{2\epsilon_s\sin^2(\omega\Delta t/2)}{3\nu^2} + \cos^2(\omega\Delta t/2)\right)^{1/2}. \tag{5.25}$$

To determine the numerical dispersion relation for the finite element scheme FEM-D2, described in Section 3.2.2, we substitute (4.10) in the discrete equations (3.20). Following the procedure discussed above we obtain the numerical dispersion relation for the FEM-D2 scheme to be

$$\sin^2(k_\Delta\Delta z/2) = \alpha^2\left(\frac{2\sin(\eta)\mathrm{i} - \lambda\cos(\eta)\epsilon_s\Delta t + \frac{1}{4}h_\tau^3\cos(\eta)\epsilon_d}{2\sin(\eta)\mathrm{i} - \lambda\cos(\eta)\epsilon_s\Delta t\beta^2\alpha^2 + \frac{1}{6}h_\tau^3\cos(\eta)\epsilon_d\alpha^2}\right), \tag{5.26}$$

where $\eta = \frac{\omega\Delta t}{2}$, $\epsilon_d = \epsilon_s - 1$ and $h_\tau = \Delta t/\tau$. If we neglect terms in h_τ^3, then the expression (5.26) reduces to (5.18). Thus, for small h_τ, both the finite element methods, FEM-D1 and FEM-D2 have the same numerical dispersion relations. From the section on stability analysis we have seen that for low dissipation h_tau needs to be about 0.001 for Debye media and 0.01 for Lorentz media. For these values of h_τ both finite element schemes produce the

same dispersion graphs (see [5]). Therefore, in the rest of this section we will consider only FEM-D1, and may refer to it as *the finite element scheme* for the Debye model. Similarly, it was shown in [29] that the phase error properties for the two FDTD methods JHT-D [19] and KF-D [21] are identical. Therefore, in the remainder of this section we will consider only JHT-D, and may refer to it as *the finite difference scheme* for the Debye model. We will compare dispersion properties of the finite element scheme FEM-D1 with those of the finite difference scheme JHT-D.

The FEM-D1 scheme misrepresents the continuous model parameters λ and ϵ_s discretely as λ_Δ and $\epsilon_{s,\Delta}$, and misrepresents the frequency ω as ω_Δ. We note that as ν increases ($\nu > \sqrt{\epsilon_s}$),the product $\alpha\beta \to 1$, and $\epsilon_{s,\Delta} \to \epsilon_s$. The discrete parameter λ_Δ for the finite element method FEM-D1 is a function of the continuous model parameter ϵ_s via the quantity β. However, for the regime of interest, namely $\omega\Delta t$ small, and when ν is large ($\nu > \sqrt{\epsilon_s}$), $2\epsilon_s \sin^2(\omega\Delta t/2)/3\nu^2$ is dominated by $\cos^2(\omega\Delta t/2)$. Also the product $\alpha\beta \to 1$, $\alpha \to 1/\cos(\omega\Delta/2)$ and thus $\lambda_\Delta \to \lambda$. Finally for $\omega\Delta t$ small and ν large, $s_\omega\alpha \approx 1$ and thus $\omega_\Delta \to \omega$. Hence, the choice of the Courant number ν is important in maintaining low dispersion error in the FEM schemes.

We compare the FEM-D1 scheme for Debye media with the finite difference scheme JHT-D presented in [19] and analyzed in [29]. The numerical dispersion relation for this finite difference scheme is given to be

$$k_\Delta = k^{\mathrm{D}}_{\mathrm{FD}}(\omega) = \frac{2}{\Delta z}\sin^{-1}\left[\frac{\omega}{c}s_\omega\frac{\Delta z}{2}\sqrt{\epsilon^{\mathrm{D}}_{r,\mathrm{FD}}}\right], \tag{5.27}$$

$$\epsilon^{\mathrm{D}}_{r,\mathrm{FD}} = \frac{\epsilon_s\lambda_\Delta - i\omega_\Delta}{\lambda_\Delta - i\omega_\Delta}. \tag{5.28}$$

If written in the form of (5.18), this would correspond to discrete representations of the continuous model parameters given as

$$\epsilon_{s,\Delta} = \epsilon_s \tag{5.29}$$

$$\lambda_\Delta = \lambda\cos(\omega\Delta t/2), \tag{5.30}$$

and a representation of the frequency by

$$\omega_\Delta = \omega s_\omega. \tag{5.31}$$

We compare the phase error for the FEM-D1 to phase error for the JHT-D scheme. The phase error is plotted against values of $\omega\Delta t$ in the range $[0, \pi]$. We note that $\omega\Delta t = 2\pi/N_{\mathrm{ppp}}$, where N_{ppp} is the number of points per period and is related to the number of points per wavelength N_{ppw} via

$$N_{\mathrm{ppw}} = \nu N_{\mathrm{ppp}}. \tag{5.32}$$

Thus, for $\nu \leq 1$, the number of points per wavelength is always less than or equal to the number of points per period, and conversely for $\nu > 1$. Note that the number of points per wavelength in the range $[\pi/4, \pi]$ is 8 to 2 points per period. We are more interested in the range $[0, \pi/4]$ which involves more than 8 points per period (or equivalently more than 8 points per wavelength).

To generate the plots below we have used the values given in (4.21), namely: $\epsilon_\infty = 1$, $\epsilon_s = 78.2$, and $\tau = 8.1 \times 10^{-12}$. Figure 8 plots the phase error Φ versus $\omega\Delta t$ for the FEM-D1 scheme (left), and the log of the phase error versus ω (right), using $h_\tau = 0.001$ and various values of ν. In Figure 8 (right) we can see that in the finite element scheme, for a fixed frequency, the phase error reduces as ν increases, even beyond 1. Figure 9 depicts the corresponding plots for the JHT-D method (recall JHT-D is conditionally stable for $\nu \leq 1$).

The report [5] contains plots of the real and imaginary parts of the relative complex permittivity for Debye media corresponding to the continuous equations (exact values), the FEM-D1 scheme with $\nu \in \{\sqrt{1/2}, 1, 4\}$, $h_\tau \in \{0.1, 0.01\}$, and finally the JHT-D scheme with $\nu \in 1$ fixed and $h_\tau \in \{0.1, 0.01\}$. Figure 10 depicts a representative example. For $h_\tau = 0.1$, as ν is increased the discrete permittivities of the finite element scheme approach the exact values. For $h_\tau = 0.01$, the agreement of the discrete permittivities with the exact values is better than with $h_\tau = 0.1$, for each value of ν. For $\nu = 4$ we see the best agreement of the discrete real and imaginary permittivities with the exact values.

This is also seen in the plots of the discrete values of the parameters λ and ϵ_s in [5]. The discrete parameters in the FEM-D1 scheme have better agreement with the exact values as ν increases and h_τ decreases. For the particular values tested there, it appears that the value of ν that correctly represents λ will sufficiently model the entire complex permittivity for many frequencies. However the discrete value of the frequency ω for the FEM-D1, as shown in Figure 11, appears to have a better agreement with the exact value when $\nu = 1$, even better than the finite difference scheme. For the JHT-D scheme, the discrete parameters do not depend on the value of ν. Still, as h_τ is decreased they do converge toward the exact values.

5.0.3 Lorentz Media

The dispersion relation for the continuous Lorentz model is given by

$$k_{\mathrm{EX}}^{\mathrm{L}}(\omega) = \frac{\omega}{c}\sqrt{\epsilon_r^{\mathrm{L}}(\omega)}. \tag{5.33}$$

where the relative complex permittivity for Lorentz media is given to be

$$\epsilon_r^{\mathrm{L}}(\omega) = \frac{\omega^2 - \epsilon_s\omega_0^2 + i\lambda\omega}{\omega^2 - \omega_0^2 + i\lambda\omega}, \tag{5.34}$$

To determine the numerical dispersion relation for the finite element method applied to a Lorentz medium (FEM-L) described in Section 3.2.3, we substitute

$$X_j^n = \begin{bmatrix} e_j^n \\ p_j^n \\ d_j^n \\ q_j^n \end{bmatrix} = \begin{bmatrix} \tilde{e} \\ \tilde{p} \\ \tilde{d} \\ \tilde{q} \end{bmatrix} \mathrm{e}^{i(k_\Delta j\Delta z - \omega n\Delta t)} \tag{5.35}$$

into the discrete equations (3.22),(3.23) and (3.24). Again, we assume that $\epsilon_\infty = 1$ in our analysis.

As before we obtain a homogeneous system of the type $\mathcal{A}\tilde{\mathcal{X}} = 0$. We then set $\det(\mathcal{A}) = 0$ to obtain a relation between the numerical wavenumber k_Δ and the frequency ω. Solving for

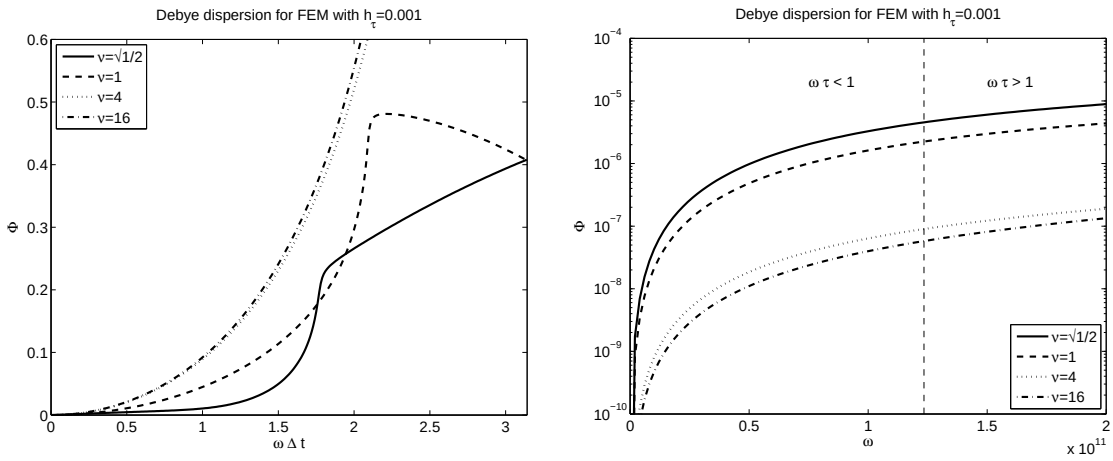

Figure 8: Plot on left (right) is of the phase error Φ (resp., log of Φ) versus $\omega\Delta t$ (resp., ω) for the FEM-D1 scheme with $\nu \in \{\sqrt{1/2}, 1, 4, 16\}$ using $h_\tau = 0.001$.

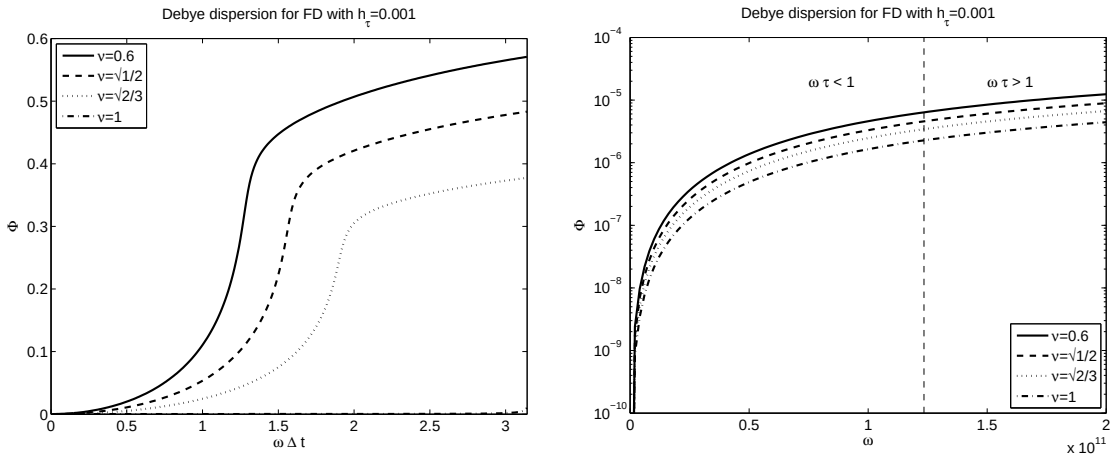

Figure 9: Plot on left (right) is of the phase error Φ (resp., log of Φ) versus $\omega\Delta t$ (resp., ω) for the JHT-D scheme with $\nu \in \{1, \sqrt{2/3}, \sqrt{1/2}, .6\}$ using $h_\tau = 0.001$.

k_Δ in this relation, and writing in a form comparable to (5.33), we have that the numerical dispersion relation for the FEM-L scheme is

$$k_\Delta = k_{\mathrm{FE}}^{\mathrm{L}}(\omega) = \frac{2}{\Delta z} \sin^{-1}\left[\frac{\omega_\Delta}{c}\frac{\Delta z}{2}\sqrt{\epsilon_{r,\mathrm{FE}}^{\mathrm{L}}}\right], \tag{5.36}$$

where the discrete relative complex permittivity is given to be

$$\epsilon_{r,\mathrm{FE}}^{\mathrm{L}} = \frac{\omega_\Delta^2 - \epsilon_{s,\Delta}\omega_{0,\Delta}^2 + i\lambda_\Delta\omega_\Delta}{\omega_\Delta^2 - \omega_{0,\Delta}^2 + i\lambda_\Delta\omega_\Delta}. \tag{5.37}$$

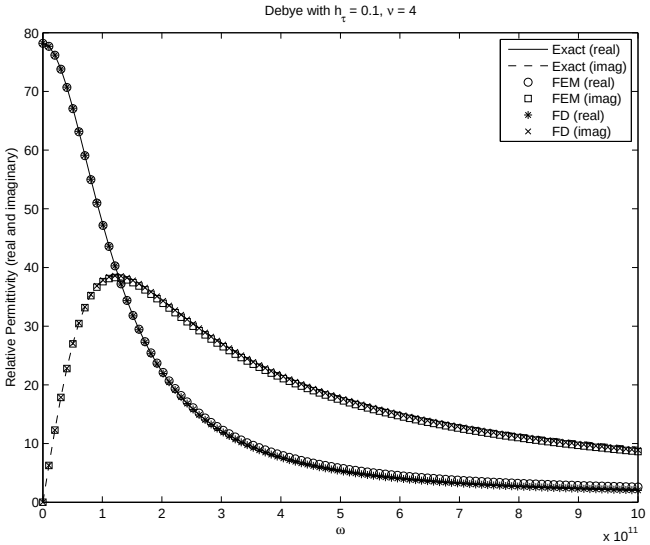

Figure 10: Plots of the real and imaginary parts of the relative complex permittivity for Debye media corresponding to the continuous equations, the FEM-D1 scheme with $\nu = 4, h_\tau = 0.1$ and the JHT-D scheme with $\nu = 1, h_\tau = 0.1$.

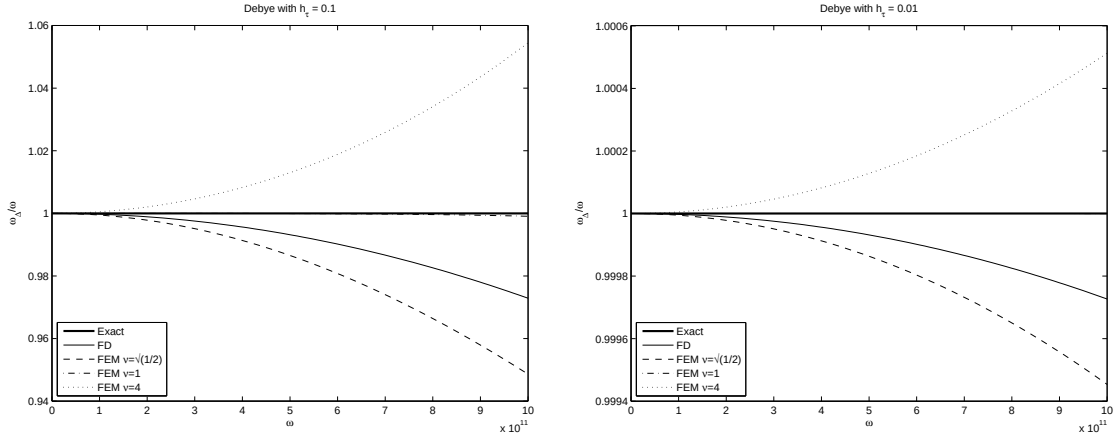

Figure 11: Plots of the frequency ω for Debye media corresponding to the continuous equations, the FEM-D1 scheme and the JHT-D scheme (using $\nu = 1$) with $h_\tau = 0.1$ (left) and $h_\tau = 0.01$ (right).

Here

$$\epsilon_{s,\Delta} = \frac{\epsilon_s}{\alpha^2\beta^2} \tag{5.38}$$

$$\lambda_\Delta = \lambda \cos(\omega\Delta t/2)\alpha \tag{5.39}$$

$$\omega_{0,\Delta} = \omega_0 \cos(\omega\Delta t/2)\beta\alpha^2 \tag{5.40}$$

$$\omega_\Delta = \omega s_\omega \alpha, \tag{5.41}$$

where s_ω, α, β are as defined in equations (5.23)–(5.25). Thus, the FEM-L scheme misrepresents ϵ_s, λ, ω_0 and ω as $\epsilon_{s,\Delta}$, λ_Δ, $\omega_{0,\Delta}$ and ω_Δ respectively. In particular, note that for the finite element method applied to the Lorentz model, λ_Δ does not depend on the continuous model parameter ϵ_s, however, $\omega_{0,\Delta}$ does. In the FEM-D1 scheme for the Debye model, λ_Δ depended on β^2, whereas in the FEM-L scheme for the Lorentz model, $\omega_{0,\Delta}$ depends directly on β. This discrete parameter appears as $\omega_{0,\Delta}^2$ in the dispersion relation, so the contribution from β is again raised to the second power. This coupled with the fact that the regime of interest $\omega\Delta t$ is small implies that as before the effect of ϵ_s on the dispersion caused by the $\omega_{0,\Delta}$ term is likely to be small.

We compare the FEM-L scheme with two different finite difference schemes which have been analyzed in [29]. For the JHT-L scheme in [19] the numerical dispersion relation is given as

$$k_\Delta = k_{\mathrm{JHT}}^{\mathrm{L}}(\omega) = \frac{2}{\Delta z}\sin^{-1}\left[\frac{\omega}{c}\frac{\Delta z}{2}s_\omega\sqrt{\epsilon_{r,\mathrm{JHT}}^{\mathrm{L}}}\right], \tag{5.42}$$

where the discrete relative complex permittivity for the JHT-L scheme is

$$\epsilon_{r,\mathrm{JHT}}^{\mathrm{L}} = \frac{\omega_\Delta^2 - \epsilon_{s,\Delta}\omega_{0,\Delta}^2 + i\lambda_\Delta\omega_\Delta}{\omega_\Delta^2 - \omega_{0,\Delta}^2 + i\lambda_\Delta\omega_\Delta}. \tag{5.43}$$

Here the discrete representations of the continuous model parameters and the frequency are given as

$$\epsilon_{s,\Delta} = \epsilon_s \tag{5.44}$$

$$\lambda_\Delta = \lambda\frac{\tilde{s}_\omega}{s_\omega} \tag{5.45}$$

$$\omega_{0,\Delta} = \omega_0\sqrt{\cos(\omega\Delta t)} \tag{5.46}$$

$$\omega_\Delta = \omega s_\omega, \tag{5.47}$$

with $\tilde{s}_\omega = \dfrac{\sin(\omega\Delta t)}{\omega\Delta t}$.

The second finite difference scheme, the KF-L scheme of [20], has a numerical dispersion relation given by

$$k_{\mathrm{KF}}^{\mathrm{L}}(\omega) = \frac{2}{\Delta z}\sin^{-1}\left[\frac{\omega}{c}\frac{\Delta z}{2}s_\omega\sqrt{\epsilon_{r,\mathrm{KF}}^{\mathrm{L}}}\right], \tag{5.48}$$

where the discrete relative complex permittivity for the KF-L scheme is

$$\epsilon_{r,\mathrm{KF}}^{\mathrm{L}} = \frac{\omega_\Delta^2 - \epsilon_{s,\Delta}\omega_{0,\Delta}^2 + i\lambda_\Delta\omega_\Delta}{\omega_\Delta^2 - \omega_{0,\Delta}^2 + i\lambda_\Delta\omega_\Delta}. \tag{5.49}$$

The discrete representations of the continuous model parameters and the frequency are given to be

$$\epsilon_{s,\Delta} = \epsilon_s \tag{5.50}$$

$$\lambda_\Delta = \lambda\cos(\omega\Delta t/2) \tag{5.51}$$

$$\omega_{0,\Delta} = \omega_0\cos(\omega\Delta t/2) \tag{5.52}$$

$$\omega_\Delta = \omega s_\omega. \tag{5.53}$$

We plot the phase error Φ as defined in (5.10) for the FEM-L and we compare it with the phase errors for the JHT-L and the KF-L finite difference schemes. The phase error is plotted against values of $\omega\Delta t$ in the range $[0, \pi]$. We note that, as before, $\omega\Delta t = 2\pi/N_{\text{ppp}}$, where N_{ppp} is the number of points per period and is related to the number of points per wavelength N_{ppw} via

$$N_{\text{ppw}} = \nu N_{\text{ppp}}. \tag{5.54}$$

To generate the plots below we have used the values for the medium parameters as given in (4.29). Figure 12 plots the phase error Φ versus $\omega\Delta t$ for the FEM-L scheme, with various values of ν and using $h_0 = 0.01$. Figures 13 and 14 plot the same for the finite difference methods JHT-L and KF-L, respectively. Figure 15 plots the phase error Φ versus ω for the FEM-L scheme, with various values of ν and using $h_0 = 0.01$. Figures 16 and 17 plot the same for the finite difference methods JHT-L and KF-L, respectively. Note that the dispersion for the finite element method reduces as ν goes to 1 for all values of h_0.

The report [5] contains plots of the real and imaginary parts of the relative complex permittivity for Lorentz media corresponding to the continuous equations (exact values), the FEM-L scheme with $\nu \in \{\sqrt{1/2}, 1, 4\}$, $h_0 \in \{0.1, 0.01\}$, and finally the KF-L scheme with $\nu = 1$ fixed and $h_0 \in \{0.1, 0.01\}$ (plots of JHT-L were similar and were thus omitted). See Figure 18 for a representative example in the case of $\nu = 1, h_0 = 0.1$. For $h_0 = 0.1$, as ν is increased, the discrete permittivities of the FEM-L scheme approach those of the KF-L method. However, for $\nu = 1$ it appears that *the finite element approximation is noticeably better*. For $h_0 = 0.01$, the agreement of the discrete permittivities with the exact values is better than with $h_0 = 0.1$, for each value of ν. For $\nu = 1$ we see the best agreement of the discrete real and imaginary permittivities with the exact values, regardless of h_0. This is not seen in the plots of the discrete values of the parameters λ, ϵ_s and ω_0 (for example, see Figure 19 for ω_0). The discrete parameters in the FEM-L scheme have better agreement with the exact values as ν is increased, even beyond 1. However the discrete value of the frequency ω appears to have a better agreement with the exact value when $\nu = 1$ (the plot is similar to that of Figure 11 for the Debye case, and therefore is omitted). As the discrete complex permittivity matches the exact more closely when $\nu = 1$, we conclude that for the Lorentz model, the value of ν that correctly represents ω will sufficiently model the complex permittivity. For the finite difference schemes, the discrete parameters do not depend on the value of ν. However, as with the finite element method FEM-L, if h_0 is decreased all discrete parameters agree better with the exact values. It should be noted that for the FEM-L scheme, as ν increases, the discrete parameters actually converge toward the KF-L values for fixed h_τ. Thus, if h_τ is too large for the KF-L values to have converged, the FEM-L scheme may actually have better agreement with the continuous values. This is precisely what is occurring in Figure 18.

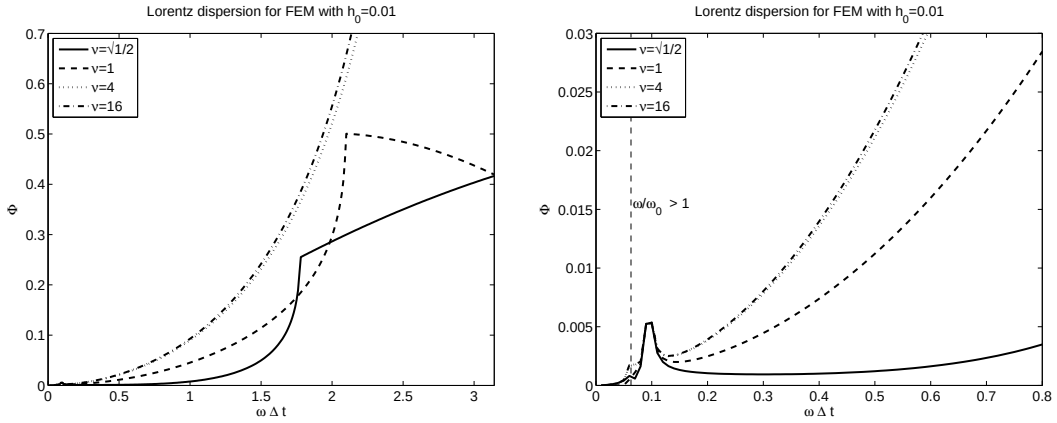

Figure 12: Plot of the phase error Φ versus $\omega\Delta t$ for the FEM-L scheme with $\nu \in \{1, \sqrt{2/3}, \sqrt{1/2}, .6\}$ using $h_0 = 0.01$. (Right plot is zoom of left.)

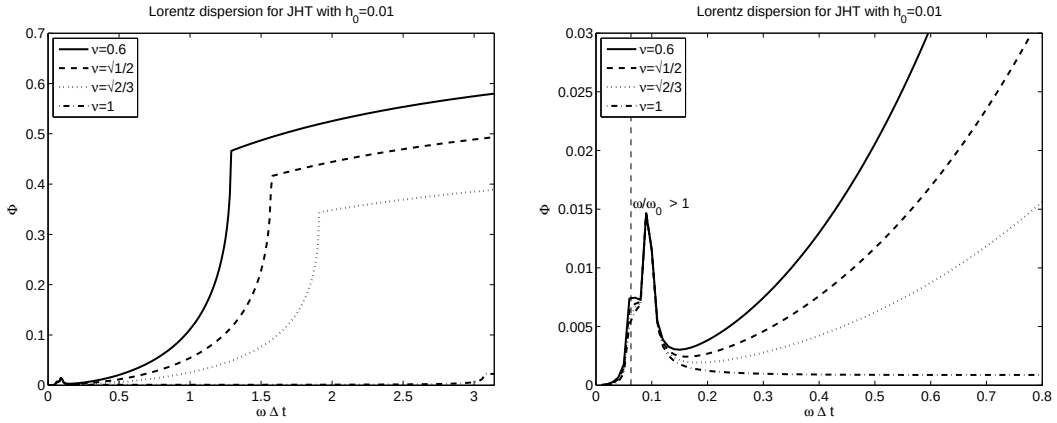

Figure 13: Plot of the phase error Φ versus $\omega\Delta t$ for the JHT-L scheme with $\nu \in \{1, \sqrt{2/3}, \sqrt{1/2}, .6\}$ using $h_0 = 0.01$. (Right plot is zoom of left.)

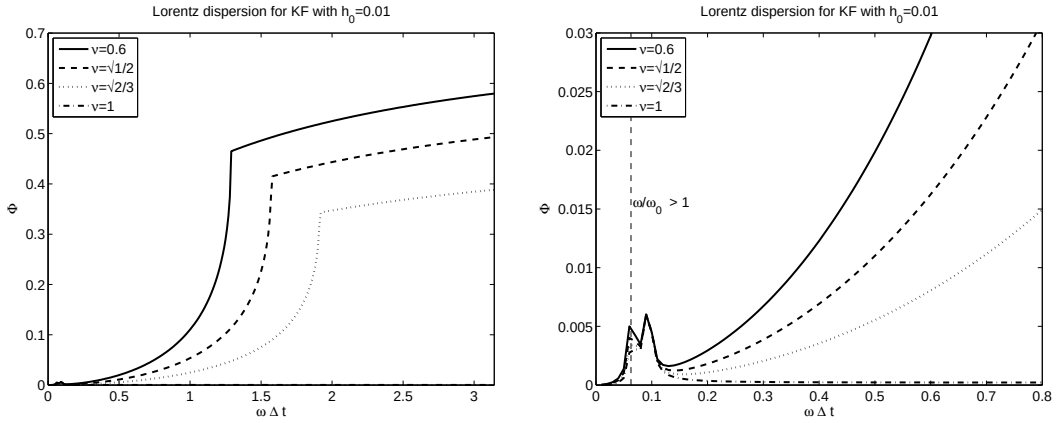

Figure 14: Plot of the phase error Φ versus $\omega\Delta t$ for the KF-L scheme with $\nu \in \{1, \sqrt{2/3}, \sqrt{1/2}, .6\}$ using $h_0 = 0.01$. (Right plot is zoom of left.)

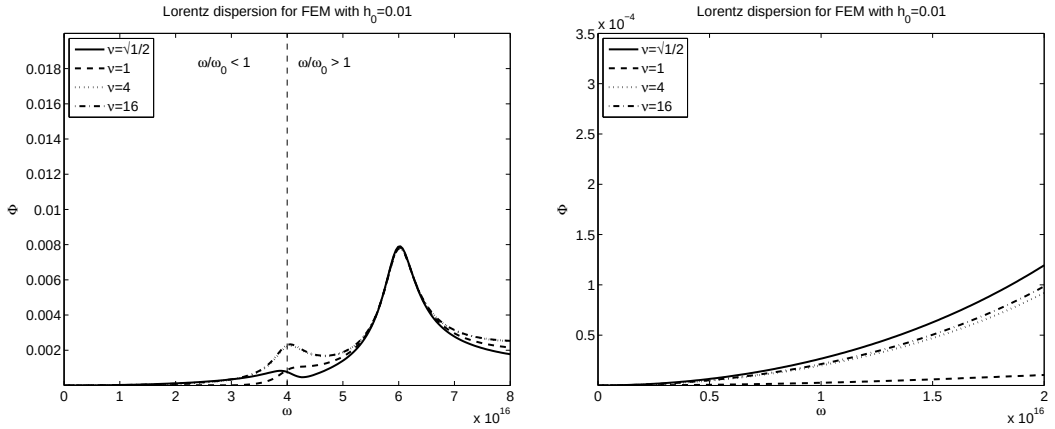

Figure 15: Plot of the phase error Φ versus ω for the FEM-L scheme with $\nu \in \{1, \sqrt{2/3}, \sqrt{1/2}, .6\}$ using $h_0 = 0.01$. (Right plot is zoom of left.)

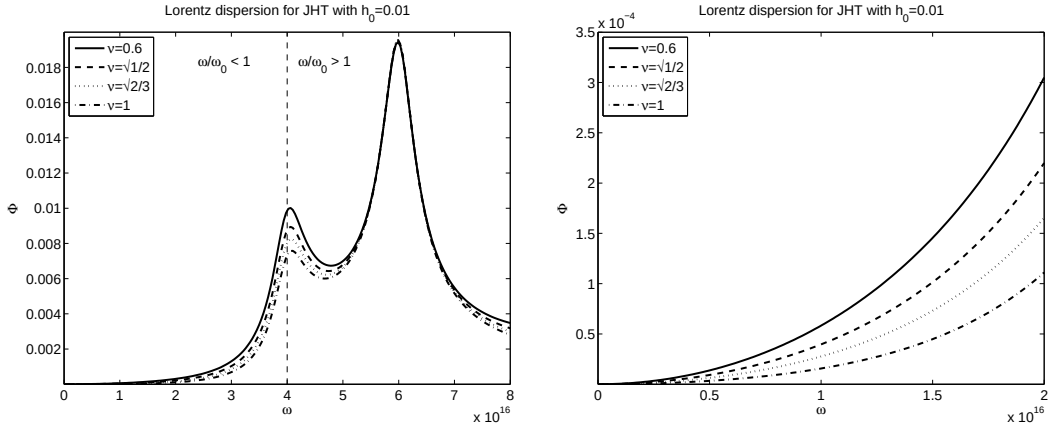

Figure 16: Plot of the phase error Φ versus ω for the JHT-L scheme with $\nu \in \{1, \sqrt{2/3}, \sqrt{1/2}, .6\}$ using $h_0 = 0.01$. (Right plot is zoom of left.)

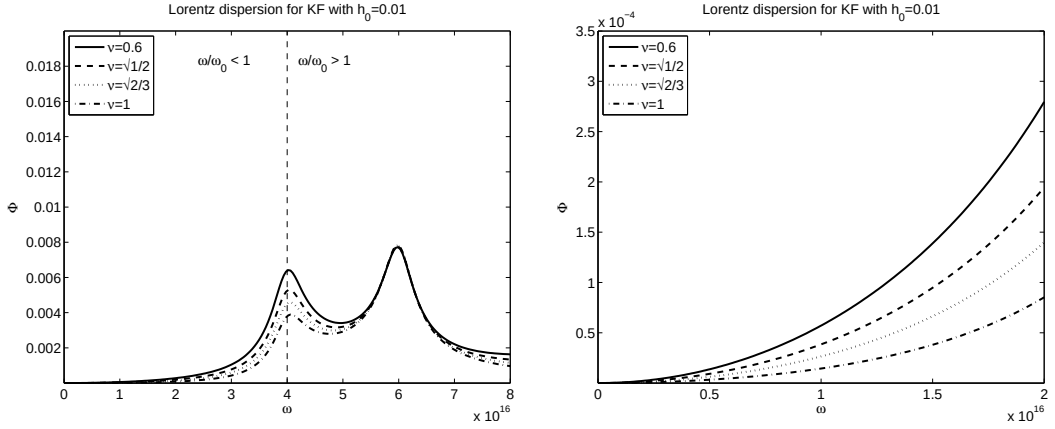

Figure 17: Plot of the phase error Φ versus ω for the KF-L scheme with $\nu \in \{1, \sqrt{2/3}, \sqrt{1/2}, .6\}$ using $h_0 = 0.01$. (Right plot is zoom of left.)

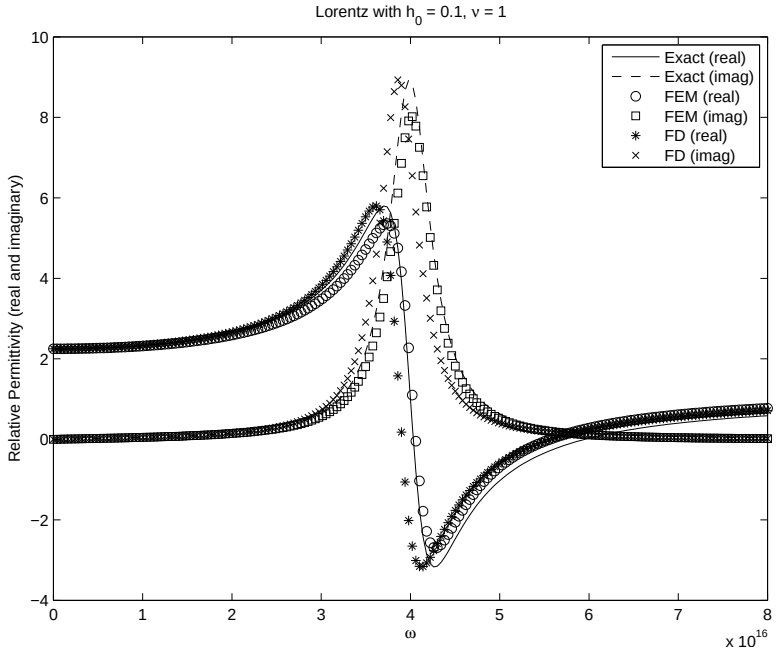

Figure 18: Plots of the real and imaginary parts of the relative complex permittivity for Lorentz media corresponding to the continuous equations, the FEM-L scheme with $\nu = 1, h_0 = 0.1$ and the KF-L scheme with $\nu = 1, h_0 = 0.1$.

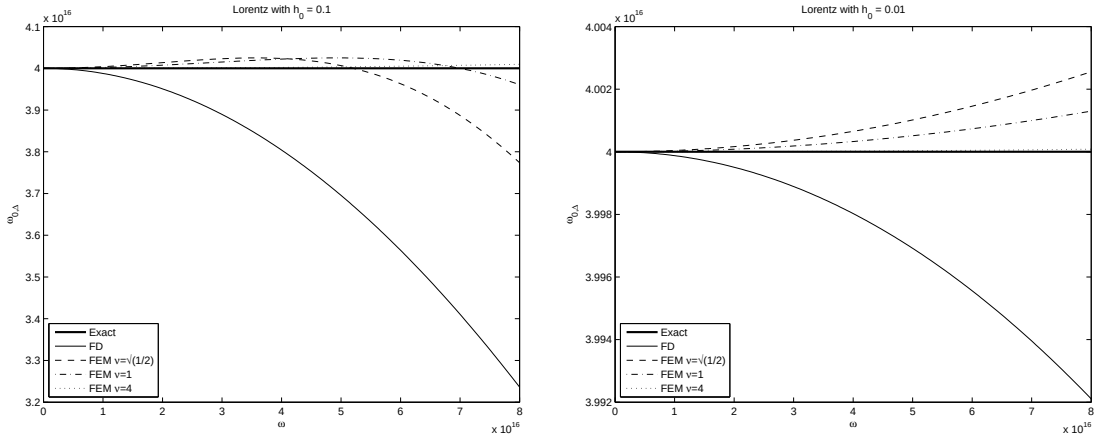

Figure 19: Plots of the resonant frequency ω_0 for Lorentz media corresponding to the continuous equations, the FEM-L scheme and the KF-L scheme (using $\nu = 1$) with $h_0 = 0.1$ (left) and $h_0 = 0.01$ (right).

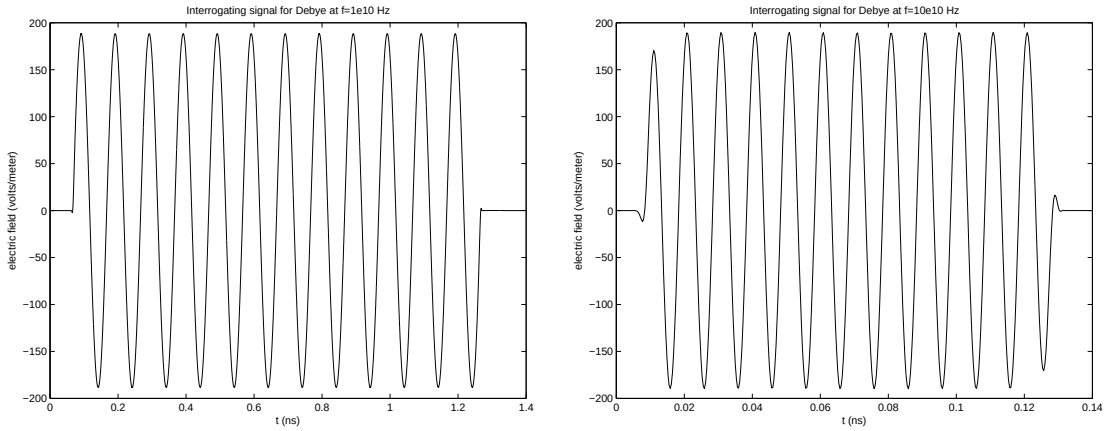

Figure 20: The interrogating signal when the carrier frequency is 10 GHz (left) and 100 GHz (right).

6 Numerical Simulations

To further compare and verify the observations drawn from the stability and dispersion analyses in the previous sections, we examine simulations of several sample problems, which use either the Debye or the Lorentz polarization model. In each case we will successively reduce the value of h_τ, and hence the time step, holding all other parameters fixed, until convergence is achieved.

6.1 Debye Simulations

In our first numerical calculation we simulate the propagation of 12 cycles of a truncated sine wave with carrier frequency at 10 GHz (1×10^{10} Hz), plotted on the left in Figure 20, which is normally incident on a Debye medium from a vacuum. The medium is defined by the parameters given in (4.21), and used subsequently throughout in all Debye computations, namely $\epsilon_s = 78.2$, $\epsilon_\infty = 1$, and $\tau = 8.1 \times 10^{-12}$ seconds. We performed simulations with the finite element scheme FEM-D2 using $\nu = 4$, as the dispersion analysis demonstrated that for this value of ν we obtained the least phase error in the regime that is of interest in this simulation. Recall that the stability and dispersion properties are nearly identical for the two finite element methods FEM-D1 and FEM-D2, however, in practice, FEM-D2 is a faster algorithm and requires less storage.

A time trace of the electric field at a depth of 15 mm into the Debye medium was recorded. Figure 21 depicts the solutions for three different values of h_τ. The traces for $h_\tau = 0.16$ and $h_\tau = 0.08$ appear to be identical at this scale. However, the left plot of Figure 22, which displays a closer view of the central portion of the signal, demonstrates that true convergence has not been reached. The right plot of Figure 22 displays a magnification of one of the peaks from the central portion of the signal with smaller h_τ values. From this plot we can see that at most $h_\tau = 0.01$ (i.e., at least 100 points per τ) is necessary for convergence on this small scale.

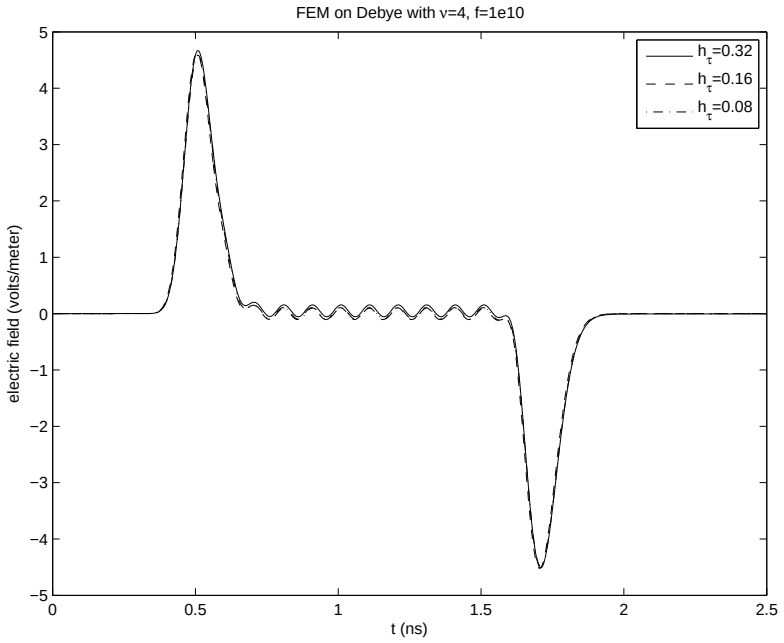

Figure 21: Time trace of the electric field at a depth of 15 mm into a Debye medium (frequency is 10 GHz) computed using the finite element scheme, for three different values of h_τ.

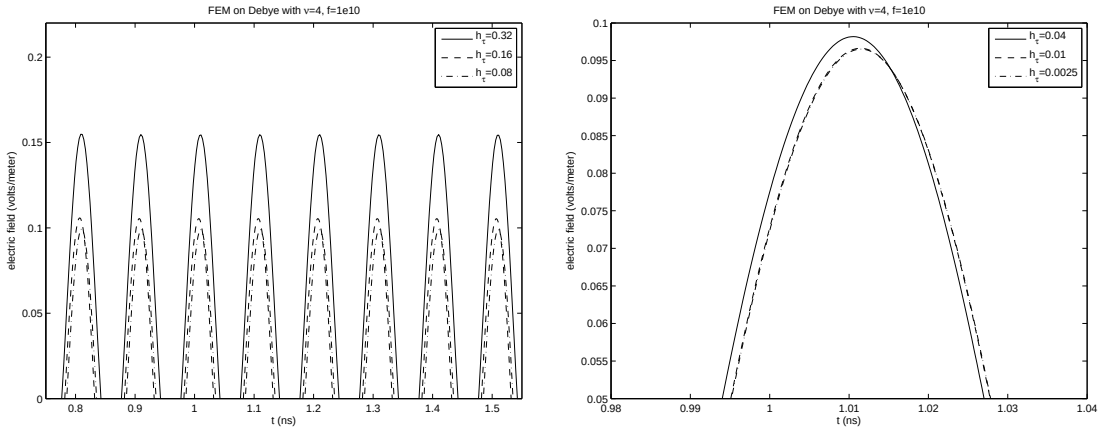

Figure 22: Closer views of the center of the time trace of the electric field at a depth of 15 mm into a Debye medium (frequency is 10 GHz), for increasingly smaller values of h_τ. (Right plot, using smaller values of h_τ, is at a finer scale than the left plot.) Convergence is achieved at $h_\tau = 0.01$.

We note that while this carrier frequency is "relatively" small (i.e., $\omega\tau = 0.5089 < 1$), and therefore the corresponding points per wavelength is large in this example ($ppw = 873$),

this high resolution of the wavelength is not the reason that the value of $h_\tau = 0.01$ is required. In fact, for an interrogating pulse with a "relatively" high carrier frequency of 100 GHz (depicted in Figure 20, right), corresponding to $\omega\tau = 5.089 > 1$, $ppw = 87.3$, we have essentially the same restriction. Plots of the signals resulting from $h_\tau = 0.01$ and $h_\tau = 0.005$ are displayed in [5], and confirm that at most $h_\tau = 0.01$ is required for convergence. In this example, the points per τ are on the same order of magnitude as the points per wavelength. Any further increase in frequency would result in the period of the interrogating signal, T, being much less than the relaxation time, and therefore choosing $h_\tau = 0.01$ would not guarantee that the smallest time scale in the problem is resolved. These examples verify the guideline of at least 100 points per relaxation time, when τ is the smallest time scale to be resolved. This is comparable to FDTD results from [29], in that to ensure minimal dispersion and dissipation error, h_τ should be less than 0.01, preferably $O(10^{-3})$.

As the same number of time steps are required for both the finite element method and the finite difference method, the fact that the finite element method used here requires a linear solve at each time step is an issue. A "fair" comparison of the stability and phase errors between the FEM-D2 and KF-D, wherein h_τ was chosen for each method in order to result in similar computational run times, was shown in [5]. The finite element method has the lesser dispersion error only for the low frequency and low resolution case. However, the stability results and phase errors for all other cases were on the same order of magnitude as the finite difference method.

6.2 Lorentz Simulations

For interrogation of a Lorentz medium, we simulate the propagation of 12 cycles of a truncated sine wave with carrier frequency at 1.5 PHz (1.5×10^{15} Hz), plotted on the left in Figure 23, which is normally incident on the medium from a vacuum. The medium is defined by the parameters given in (4.29), and used subsequently in all Lorentz computations, namely $\epsilon_s = 2.25$, $\epsilon_\infty = 1$, $\tau = 1.786 \times 10^{-16}$, and $\omega_0 = 4 \times 10^{16}$. We performed simulations with the finite element scheme, FEM-L, using $\nu = 1$.

A time trace of the electric field at a depth of 0.01 mm into the Lorentz medium was recorded. The right plot in Figure 23 depicts the solutions for three different values of h_τ. The traces for $h_0 = 0.16$ and $h_0 = 0.08$ appear to be identical at this scale. However, the left plot of Figure 24, which displays a closer view of the central portion of the signal, demonstrates that true convergence has not been reached. The right plot of Figure 24 displays a magnification of one of the peaks from the central portion of the signal computed with smaller h_0 values. From this plot we can see that at most $h_0 = 0.02$ (i.e., at least 50 points per ω_0) is necessary for convergence on this small scale. The required value of $h_0 < 0.02$ is in line with the suggested range of $O(10^{-2})$. This again is comparable to FDTD results from [29].

Again, the finite element method, FEM-L, used here requires a linear solve at each time step as opposed to both finite difference methods. The report [5] compares the stability and phase errors of the finite element method and the KF-L scheme for values of h_0 which result in comparable computational run times. As in the Debye case, the stability results and phase errors for FEM-L are all on the same order of magnitude as in the finite difference method KF-L.

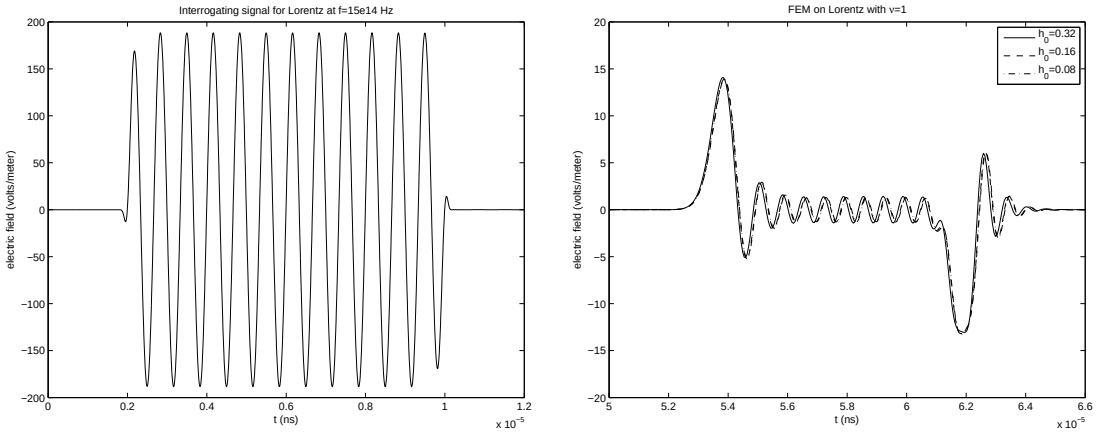

Figure 23: The interrogating signal (left) when the frequency is 1.5 PHz, and the time trace (right) of the electric field at a depth of 0.01 mm into a Lorentz medium computed using the finite element scheme, for three different values of h_0.

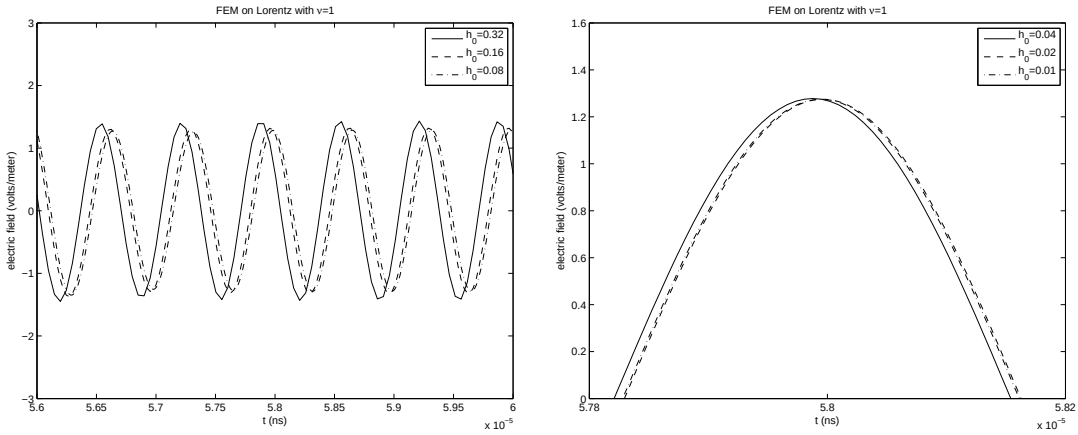

Figure 24: Closer views of the center of the time trace of the electric field at a depth of 0.01 mm into a Lorentz medium (frequency is 1.5 PHz), for increasingly smaller values of h_0. (Right plot, using smaller values of h_0, is at a finer scale than the left plot.) Convergence is achieved at $h_0 = 0.02$.

7 Conclusions

From the stability and dispersion analysis as well as the simulations shown in the paper, we can conclude that the artificial dissipation in the finite element schemes presented here for Debye and Lorentz media are strongly dependent on the quantity $h_\tau = \Delta t/\tau$ when τ is the smallest time scale. For Lorentz media, in addition, the quantity $h_0 = \Delta t/T_0$ may be the dominant quantity if $T_0 = 2\pi/\omega_0$ is smaller than τ. We see that h_τ or h_0 have to be sufficiently small in order to accurately model the propagation of pulses at large distances inside the dispersive dielectric medium. For Debye media h_τ is recommended to be at least 100 points per τ, preferably $h_\tau = O(10^{-3})$. For Lorentz media we recommend either h_0 or h_τ to be $O(10^{-2})$ in order to minimize dissipation. These results are comparable to the guidelines for FDTD schemes posed in [29].

From the dispersion analysis for the finite element schemes we see that the value of the Courant number ν to be preferred is the one that provides the best agreement of the discrete relative complex permittivity with the exact permittivity, i.e., the value that results in the least phase error for the regime of interest. The unconditional stability of the finite element scheme allows the user to have some freedom in the choice of ν. For the Debye model, the value of ν that results in the best discrete representation of $\lambda = 1/\tau$ should sufficiently approximate the complex permittivity. For the Lorentz model, the value of ν that correctly represents the angular frequency ω should be chosen.

To conclude, we have provided an analysis and representative simulations of finite element schemes for modeling dispersive wave propagation in complex dielectric media. We considered materials described by Debye and Lorentz polarization models, but the numerical approach is sufficiently general to allow for any model with an ODE representation. We have contrasted our analyses with those corresponding to the FDTD schemes.

There are numerous finite difference time domain schemes that have been developed and analyzed for the numerical simulation of Maxwell's equations in dispersive media. Finite difference schemes are popular due to their simplicity and ease of use, as well as satisfaction of many continuum properties at the discrete level, such as energy conservation. Uniform grids are used for spatial discretization along with explicit time discretization which eliminates the use of linear solvers. FDTD schemes are second order accurate in space and time and are conditionally stable. As has been shown in [29], the use of these schemes in dispersive media requires very small time and spatial steps in order to accurately and efficiently model wave propagation at large distances into a complex dispersive medium. The stringent restriction on the time and spatial steps, along with conditional stability, puts prohibitive restrictions on the use of these schemes for modeling dispersive electromagnetic phenomena, especially in three dimensions. In addition, the implementation of such schemes in not straightforward in the case of computational domains with complicated geometries. For modeling inclusions involving curved surfaces, the FDTD schemes employ a stair stepping approach which can be very inaccurate.

In order to avoid these difficulties, the finite element method provides an attractive alternative. Finite element approaches allow the use of general meshes that can be used to avoid stair stepping in the modeling of inclusions with complicated geometry. To this end, this paper provides a first step in the construction, implementation and analysis of finite element schemes for modeling dispersive wave phenomenon. The unconditional stability of

the presented scheme allows the choice of time step to be determined strictly with regard to resolving time scales. Finally, the numerical dispersion and dissipation errors in the finite element scheme investigated here are comparable to those for the finite difference schemes, even when the resolution is decreased in order that the computational run times be similar.

Acknowledgments

This research was supported in part by the U. S. Air Force Office of Scientific Research under grant AFOSR FA9550-04-1-0220 and in part by the National Institute of Aerospace (NIA) and NASA under grant NIA/NCSU-03-01-2536-NC.

References

[1] R. A. Albanese, H. T. Banks, and J. K. Raye. Nondestructive evaluation of materials usig pulsed microwave interrogating signals and acoustic wave induced reflections. *Inverse Problems*, 18:1935–1958, 2002.

[2] R. A. Albanese, R. L. Medina, and J. W. Penn. Mathematics, medicine and microwaves. *Inverse Problems*, 10:995–1007, 1994.

[3] R. A. Albanese, J. W. Penn, and R. L. Medina. Short-rise-time microwave pulse propagation through dispersive biological media. *J. Optical Society of America A*, 6:1441–1446, 1989.

[4] J. C. Anderson. *Dielectrics*. Chapman and Hall, London, 1967.

[5] H. T. Banks, V. A. Bokil and N. L. Gibson. Analysis of stability and dispersion in a finite element method for Debye and Lorentz dispersive media. Technical Report CRSC-TR06-20, Center for Research in Scientific Computation, August, 2006.

[6] H. T. Banks, M. W. Buksas, and T. Lin. *Electromagnetic Material Interrogation Using Conductive Interfaces and Acoustic Wavefronts*, volume FR21 of *Frontiers in Applied Mathematics*. SIAM, Philadelphia, PA, 2000.

[7] H. T. Banks and N. L. Gibson. Electromagnetic inverse problems involving distributions of dielectric mechanisms and parameters. Technical Report CRSC-TR05-29, Center for Research in Scientific Computation, August, 2005; *Quarterly of Applied Mathematics*, to appear.

[8] H. T. Banks and N. L. Gibson. Well-posedness in maxwell systems with distributions of polarization relaxation parameters. Technical Report CRSC-TR04-01, Center for Research in Scientific Computation, January, 2004; *Applied Math. Letters*, 18(4):423–430, 2005.

[9] H. T. Banks, N. L. Gibson, and W. P. Winfree. Gap detection with electromagnetic terahertz signals. Technical Report CRSC-TR03-40, Center for Research in Scientific Computation, September, 2003; *Nonlinear Analysis: Real World Applications*, 6:381–416, 2005.

[10] I. Barba, A. C. L. Cabeceira, M. Panizo, and J. Represa. Modelling dispersive dielectrics in TLM method. *Int. J. Numer. Model.*, 14:15–30, 2001.

[11] B Bidegaray-Fesquet. Stability of fd-td schemes for maxwell-debye and maxwell-lorentz equations. Technical Report LMC-IMAG 1077-M, Laboratoire de Modélisation et de Calcul, CNRS, 2005.

[12] K. S. Cole and R. H. Cole Dispersion and absorption in dielectrics. *J. Chem. Phy.*, 9:341–351, 1941.

[13] S. A. Cummer. An analysis of new and existing FDTD methods for isotropic cold plasma and a method for improving their accuracy. *IEEE Trans. Antennas Propagat.*, 45:392–400, 1996.

[14] T. A. Davis and I. S. Duff. An unsymmetric-pattern multifrontal method for sparse lu factorization. *SIAM J. Matrix Analysis and Applications*, 1997.

[15] P. Debye. *Polar Molecules.* Chemical Catalog Co., New York, 1929.

[16] F. Edelvik and B. Strand. Frequency dispersive materials for 3-d hybrid solvers in time domain. *IEEE Trans. Antennas Propagat.*, 51:1199–1205, 2003.

[17] E. C. Fear, P. M. Meaney, and M. A. Stuchly. Microwaves for breast cancer detection. *IEEE Potentials*, pages 12–18, 2003.

[18] J. D. Jackson. *Classical Electromagnetics.* John Wiley and Sons, New York, 1999.

[19] R. M. Joseph, S. C. Hagness, and A. Taflove. Direct time integration of Maxwell's equations in linear dispersive media with absorption for scattering and propagation of femtosecond electromagnetic pulses. *Optics Lett.*, 16(18):1412–1414, 1991.

[20] T. Kashiwa and I. Fukai. A treatment by the FD-TD method of the dispersive characteristics associated with electronic polarization. *Microwave Opt. Technol. Lett.*, 3(6):203–205, 1990.

[21] T. Kashiwa, N. Yoshida, and I. Fukai. A treatment by the finite-difference time domain method of the dispersive characteristics associated with orientational polarization. *IEEE Transactions of the IEICE*, 73(8):1326–1328, 1990.

[22] D. Kelley and R. Luebbers. Piecewise linear recursive convolution for dispersive media using FDTD. *IEEE Trans. Antennas Propagat.*, 44:792–797, 1996.

[23] Burden R. L. and J. D. Faires. *Numerical Analysis.* PWS, Boston, 1993.

[24] J-F. Lee, Lee Robert, and A. Cangellaris. Time-domain finite element methods. *IEEE Trans. Antennas Propagat.*, 45:430–442, 1997.

[25] R Lee and A. C. Cangellaris. A study of discretization error in the finite element approximation of wave solutions. *IEEE Trans. Antennas Propagat.*, 40:542–549, 1992.

[26] R. Luebbers and F. P. Hunsberger. FDTD for Nth-order dispersive media. *IEEE Trans. Antennas Propagat.*, 40:1297–1301, 1992.

[27] R. Luebbers, F. P. Hunsberger, K. S. Kunz, R. B. Standler, and M. Schneider. A frequency dependent finite-difference time-domain formulation for dispersive materials. *IEEE Trans. Electromag. Compat.*, 32:222–227, 1990.

[28] Peter Monk. A comparison of three mixed methods for the time-dependent Maxwell's equations. *SIAM J. Sci. Stat. Comput.*, 13(5):1097–1122, 1992.

[29] P. Petropoulos. Stability and phase error analysis of FDTD in dispersive dielectrics. *IEEE Trans. Antennas Propagat.*, 42(1):62–69, 1994.

[30] K. P. Prokopidis, E. P. Kosmidou, and T. D. Tsiboukis. An fdtd algorithm for wave propagation is dispersive media using higher-order schemes. *J. Electromagnetic Waves Appl.*, 18:1171–1194, 2004.

[31] R. Siushansian and LoVetri J. A comparison of numerical techniques for modeling electromagnetic dispersive media. *IEEE Microwave Guided Wave Lett.*, 5:426–428, 1995.

[32] N. S. Stoykov, T. A. Kuiken, M. M. Lowery, and A. Taflove. Finite element time-domain algorithms for modeling linear Debye and Lorentz dielectric dispersions at low frequencies. *IEEE Trans. Biomed. Enggr.*, 50:1100–1106, 2003.

[33] J. C. Strikverda. *Finite Difference Schemes and Partial Differential Equations*. SIAM, 2004.

[34] D. Sullivan. A frequency-dependent FDTD method for biological applications. *IEEE Trans. Microwave Theory*, 40:532–539, 1992.

[35] D. Sullivan. Z-transform theory and the fdtd method. *IEEE Trans. Antennas Propagat.*, 44:28–34, 1996.

[36] A. Taflove. *Computational Electrodynamics: The Finite-Difference Time-Domain method*. Artech House, Norwood, MA, 1995.

[37] A. Taflove and S. C. Hagness. *Computational Electrodynamics: The Finite-Difference Time-Domain method*. Artech House, Norwood, MA, 3rd edition, 2005.

[38] J. L. Young and R. O. Nelson. A summary and systematic analysis of fdtd algorithms for linearly dispersive media. *IEEE Antennas and Propagation Magazine*, 43:61–77, 2001.